AD-A153 494 THE EFFECT OF CENTER DELAMINATION ON THE INSTABILITY OF 1/1
COMPOSITE CYLINDRICAL PANELS(U) AIR FORCE INST OF TECH
WRIGHT-PATTERSON AFB OH SCHOOL OF ENGI.. G R SEIFERT
UNCLASSIFIED DEC 84 AFIT/GAE/AA/84D-25 F/G 11/4 NL

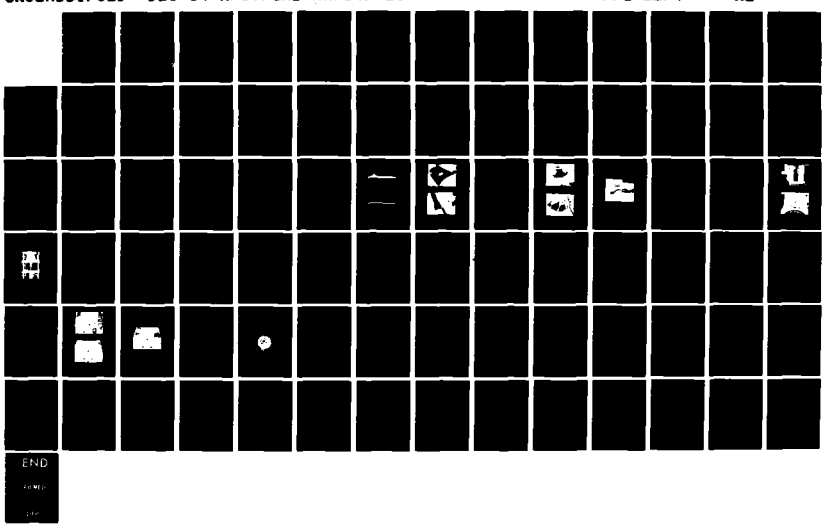

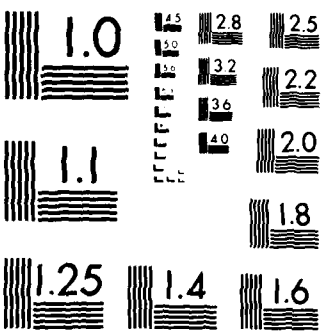

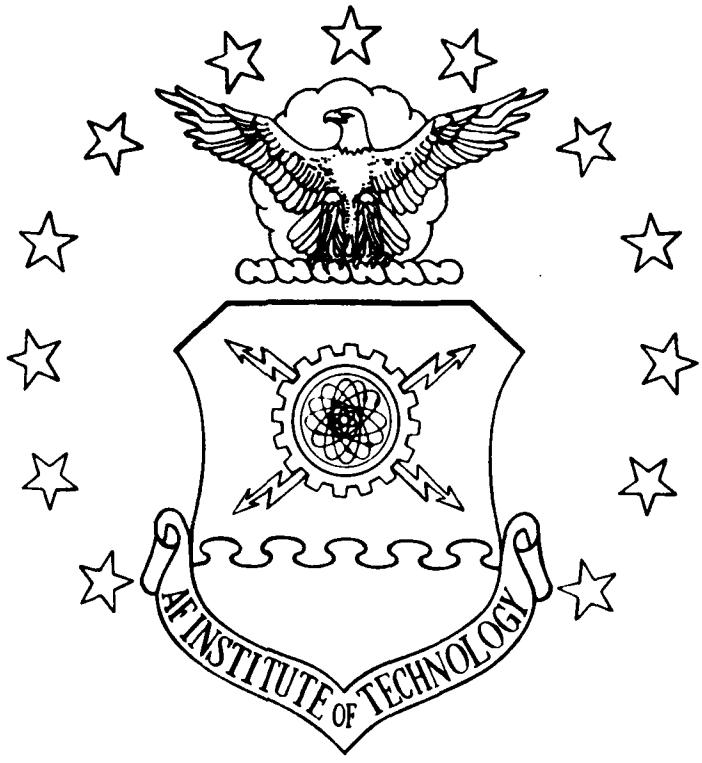

DEPARTMENT OF THE AIR FORCE

AIR UNIVERSITY

AIR FORCE INSTITUTE OF TECHNOLOGY

Wright-Patterson Air Force Base, Ohio

AFIT/GAE/AA/84D-25

THE EFFECT OF CENTER DELAMINATION ON THE INSTABILITY OF COMPOSITE CYLINDRICAL PANELS

THESIS

Gary R. Seifert
Captain, USAF

AFIT/GAE/AA/84D-25

Approved for public release; distribution unlimited

AFIT/GAE/AA/84D-25

THE EFFECT OF CENTER DELAMINATION ON THE INSTABILITY OF COMPOSITE CYLINDRICAL PANELS

THESIS

Presented to the Faculty of the School of Engineering
of the Air Force Institute of Technology
Air University (AU)
In Partial Fulfillment of the
Requirements for the Degree of
Master of Science

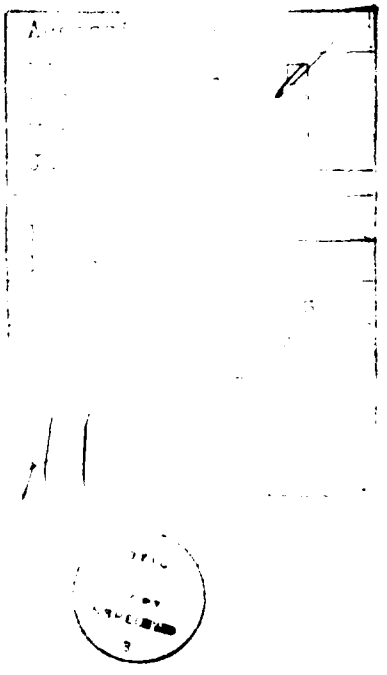

by
Gary R. Seifert
Captain, USAF

December 1984

Acknowledgments

I wish to express my sincere gratitude to Dr. Anthony N. Palazotto for his patience and professional guidance throughout all phases of this thesis. Also, I would like to thank the Air Force Flight Dynamics Laboratory for their support and funding needed to conduct the experimentation.

Most of all, I wish to thank my wife, Sherry, my daughter, Jenny, and sons, Daniel and Michael, who through their love and support insured this project was completed.

Table of Contents

List of Symbols

E_1	Longitudinal Modulus of Elasticity
E_2	Transverse Modulus of Elasticity
G_{12}	Shear Modulus
υ	Poissons' Ratio
u,v,w	Displacements in x,y,z directions, respectively
w,x	Comma denotes partial differentiation
t	Panel Thickness
R	Panel Radius of Curvature
C	Panel Chord Length
L	Panel Length
x,y,z	Structural Coordinate Directions
θ	Ply Orientation
Q_{ij}	Reduced Stiffness
$\bar{Q}_{ij}$	Transformed Reduced Stiffness
A_{ij}	Extensional Stiffness
B_{ij}	Coupling Stiffness
D_{ij}	Bending Stiffness
1,2,3	Lamina Principal Axis Directions
z	Distance From Panel Midsurface
σ	Normal Stress
τ	Shear Stress
ϵ	Direct Strain
γ	Shear Strain

K	Curvature
N_x, N_y, N_{xy}	Force Resultants
M_x, M_y, M_{xy}	Moment Resultants
ρ	Ratio of Bending Strain Versus Membrane Strain
a	Delamination Radius
$\tilde{a}$	Non-dimensionalized Delamination Radius
$\tilde{G}\tilde{a}^4$	Non-dimensionalized Energy-Release Rate

List of Figures

List of Tables

Abstract

The buckling loads of 8-ply graphite-epoxy delaminated cylindrical panels were determined experimentally. The analysis included two different ply orientations, two different aspect ratios (length/chord), two different delamination sizes, and one set of boundary conditions; clamped along the top and bottom edges and simply supported along the vertical sides. The experimental test results were compared to the linear bifurcation loads obtained from the STAGSC-1 finite element computer code and the buckling loads of panels with square cutouts which were also obtained from STAGSC-1.

The experimental testing was accomplished by the Air Force Flight Dynamics Laboratory. Experimental difficulties were encountered due to the inability of the test apparatus to evenly distribute the load through the simply supported boundary conditions. The uneven load distribution resulted in nonsymmetric buckling patterns, however, the buckling loads showed good correlation between analytical and experimental values. All experimental buckling loads were less than the analytical value predicted by STAGSC-1. The amount of decrease in load depended on ply orientation, aspect ratio, and delamination size.

Equations (9) and (10) are expanded for an N-layered laminate as:

$$\begin{Bmatrix} N_x \\ N_y \\ N_{xy} \end{Bmatrix} = \int_{-t/2}^{t/2} \begin{Bmatrix} \sigma_x \\ \sigma_y \\ \tau_{xy} \end{Bmatrix} dz = \begin{Bmatrix} \sum_{k=1}^{N} \end{Bmatrix} \int_{z_{k-1}}^{z_k} \begin{Bmatrix} \sigma_x \\ \sigma_y \\ \tau_{xy} \end{Bmatrix} dz \qquad (11)$$

and

$$\begin{Bmatrix} M_x \\ M_y \\ M_{xy} \end{Bmatrix} = \int_{-t/2}^{t/2} \begin{Bmatrix} \sigma_x \\ \sigma_y \\ \tau_{xy} \end{Bmatrix} z dz = \sum_{k=1}^{N} \int_{z_{k-1}}^{z_k} \begin{Bmatrix} \sigma_x \\ \sigma_y \\ \tau_{xy} \end{Bmatrix} z dz \qquad (12)$$

where z_k and z_{k-1} are defined in Fig. 4.

By substituting Equation (8) into Equations (11) and (12) and recalling the stiffness matrix, $\bar{Q}_{ij}$ is constant within a lamina, the integration is simplified by pulling the stiffness matrix outside the integration. The stiffness matrix is summed over each layer and Equations (11) and (12) are rewritten as:

$$\begin{Bmatrix} N_x \\ N_y \\ N_{xy} \end{Bmatrix} = \sum_{k=1}^{N} [\bar{Q}]_k \left[\int_{z_{k-1}}^{z_k} \begin{Bmatrix} \epsilon_x^0 \\ \epsilon_y^0 \\ \gamma_{xy}^0 \end{Bmatrix} dz + \int_{z_{k-1}}^{z_k} \begin{Bmatrix} K_x \\ K_y \\ K_{xy} \end{Bmatrix} z dz \right] \qquad (13)$$

and

$$\begin{Bmatrix} M_x \\ M_y \\ M_{xy} \end{Bmatrix} = \sum_{k=1}^{N} [\bar{Q}]_k \left[\int_{z_{k-1}}^{z_k} \begin{Bmatrix} \epsilon_x^0 \\ \epsilon_y^0 \\ \gamma_{xy}^0 \end{Bmatrix} z dz + \int_{z_{k-1}}^{z_k} \begin{Bmatrix} K_x \\ K_y \\ K_{xy} \end{Bmatrix} z^2 dz \right] \qquad (14)$$

$$N_x = \int_{-t/2}^{t/2} \sigma_x dz \tag{9}$$

and

$$M_x = \int_{-t/2}^{t/2} \sigma_x z dz \tag{10}$$

The resultant forces and moments per unit length on a cross section of a laminate are shown in Fig. 5.

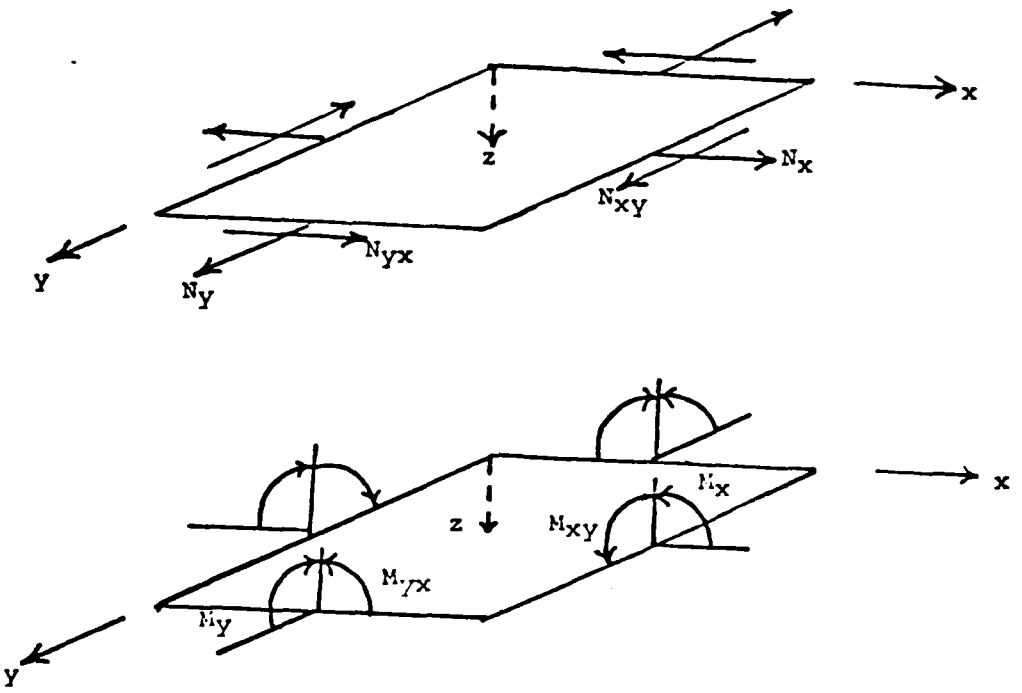

Forces and Moments on a Laminate

Figure 5

With these assumptions, the following strain-curvature relation can be written for a laminate:

$$\begin{Bmatrix} \epsilon_x \\ \epsilon_y \\ \gamma_{xy} \end{Bmatrix} = \begin{Bmatrix} \epsilon_x^0 \\ \epsilon_y^0 \\ \gamma_{xy}^0 \end{Bmatrix} + z \begin{Bmatrix} K_x \\ K_y \\ 2K_{xy} \end{Bmatrix} \tag{7}$$

where the superscript '0' indicates the mid-surface strains, z is the distance from the panel mid-surface, and K are the mid-surface curvatures. Substituting Equation (7) into Equation (4), the stress in the kth layer can be expressed in terms of the laminate middle surface strains and curvatures:

$$\begin{Bmatrix} \sigma_x \\ \sigma_y \\ \tau_{xy} \end{Bmatrix} = [\bar{Q}]_k \begin{Bmatrix} \epsilon_x^0 \\ \epsilon_y^0 \\ \gamma_{xy}^0 \end{Bmatrix} + z \begin{Bmatrix} K_x \\ K_y \\ K_{xy} \end{Bmatrix} \tag{8}$$

Once the stresses in a layer are known, the resultant forces and moments are obtained by integrating the stresses in each lamina through the total laminate thickness. The force, N_x, is expressed as a force per unit length and moment, M_x, expressed as a moment per unit length, are calculated from:

$$\bar{Q}_{16} = (Q_{11}-Q_{12}-2Q_{66})\sin\theta\cos^3\theta + (Q_{12}-Q_{22}+2Q_{66})\sin^3\theta\cos\theta$$

$$\bar{Q}_{26} = (Q_{11}-Q_{12}-2Q_{66})\sin^3\theta\cos\theta + (Q_{12}-Q_{22}+Q_{66})\sin\theta\cos^3\theta \quad \text{(5.Cont.)}$$

$$\bar{Q}_{66} = (Q_{11}+Q_{22}-2Q_{12}-2Q_{66})\sin^2\theta\cos^2\theta + Q_{66}(\sin^4\theta+\cos^4\theta)$$

The stress-strain relation defined in Equation (4) represents the relation for the k^{th} layer in a laminate:

$$\{\sigma\}_k = [\bar{Q}]_k \{\epsilon\}_k \qquad (6)$$

To use Equation (6) and expand the stress-strain relations to a multilayered laminate (Fig. 4) certain assumptions are made. First, the intralaminar bonds are considered perfect so that no lamina can slip relative to another. Second, the Kirchoff-Love hypothesis is valid and requires that sections normal to the panel's mid-surface remain plain and normal to the mid-surface after bending [16].

where E_1 and E_2 are Young's moduli in the 1 and 2 directions respectively. Poissons' ratio, υ_{ij} is the ratio of transverse strain in the j direction when loaded in the i direction. G_{12} is the shear modulus in the 1-2 plane. The values are further defined in the following relations:

$$\begin{aligned} \upsilon_{12} &= - E_2/E_1 \\ \upsilon_{21} &= - E_1/E_2 \\ G_{12} &= \tau_{12}/\gamma_{12} \end{aligned} \tag{3}$$

The preceding relations defined the strains and stresses in only the principal material directions. Common use of composites have the lamina axis oriented at some angle, θ, to the structural axis. In this case the stresses are:

$$\begin{Bmatrix} \sigma_x \\ \sigma_y \\ \tau_{xy} \end{Bmatrix} = \begin{bmatrix} \bar{Q}_{11} & \bar{Q}_{12} & \bar{Q}_{16} \\ \bar{Q}_{12} & \bar{Q}_{22} & \bar{Q}_{26} \\ \bar{Q}_{16} & \bar{Q}_{26} & \bar{Q}_{66} \end{bmatrix} \begin{Bmatrix} \epsilon_x \\ \epsilon_y \\ \gamma_{xy} \end{Bmatrix} \tag{4}$$

where $\bar{Q}_{ij}$, the transformed reduced stiffness, is defined as:

$$\begin{aligned} \bar{Q}_{11} &= Q_{11}\cos^4\theta + 2(Q_{12}+2Q_{66})\sin^2\theta\cos^2\theta + Q_{22}\sin^4\theta \\ \bar{Q}_{12} &= (Q_{11}+Q_{22}-4Q_{66})\sin^2\theta\cos^2\theta + Q_{12}(\sin^4\theta+\cos^4\theta) \\ \bar{Q}_{22} &= Q_{11}\sin^4\theta + 2(Q_{12}+2Q_{66})\sin^2\theta\cos^2\theta + Q_{22}\cos^4\theta \end{aligned} \tag{5}$$

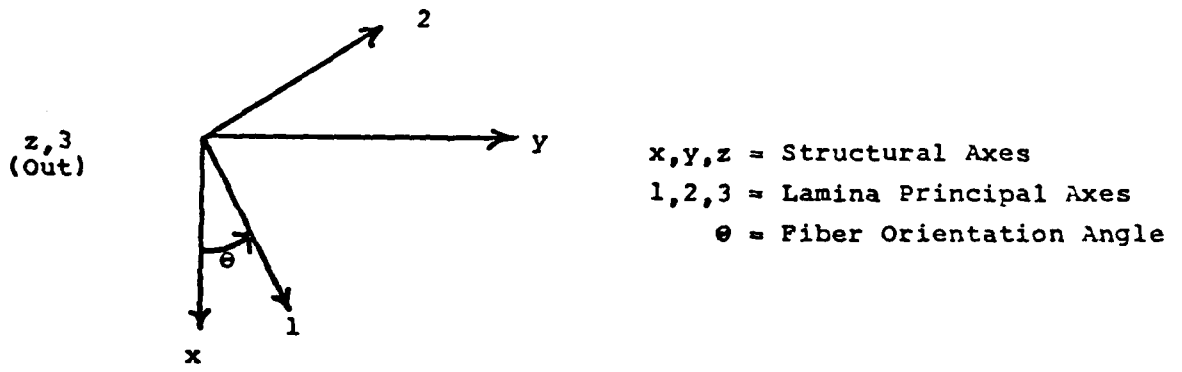

Definition of Composite Coordinate System

Figure 3

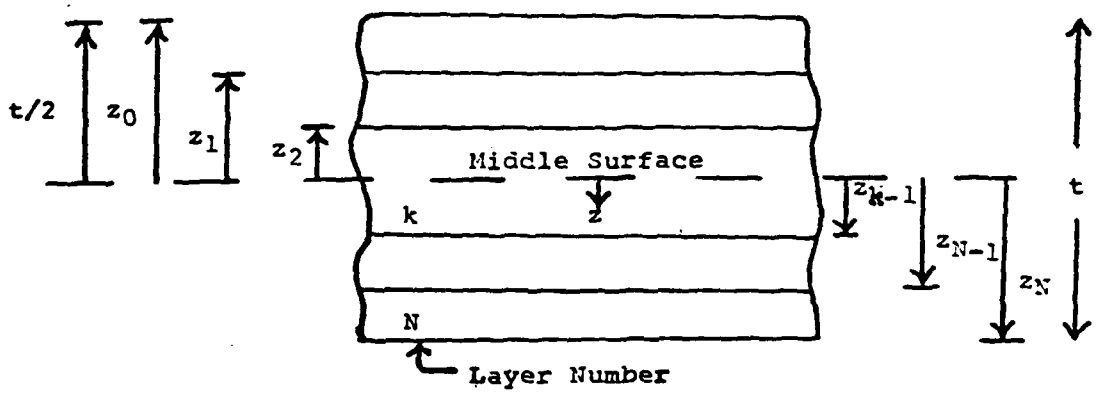

Geometry of an N Layered Laminate

Figure 4

cannot maintain equilibrium.. The lower path represents the occurrence of buckling and the usual linear load-stress-strain-deflection relations do not hold. However, the lower path represents equilibrium in the structure.

Classical Lamination Theory

In order to understand the behavior of a composite laminate, it is necessary to understand the basic constitutive relationships. References [16] and [17] present an in-depth development of these relations.

Before a complete laminate made up of N layers can be analyzed, the relations for a single lamina are presented. The stress-strain relations for the individual laminae are similar to those of an orthotropic material in plane stress. This relation in principal material coordinates (Fig. 3) is given as:

$$\begin{Bmatrix} \sigma_1 \\ \sigma_2 \\ \tau_{12} \end{Bmatrix} = \begin{bmatrix} Q_{11} & Q_{12} & 0 \\ Q_{12} & Q_{22} & 0 \\ 0 & 0 & Q_{66} \end{bmatrix} \begin{Bmatrix} \epsilon_1 \\ \epsilon_2 \\ \gamma_{12} \end{Bmatrix} \tag{1}$$

where Q_{ij} is the reduced stiffness matrix defined in terms of the engineering constants:

$$\begin{aligned} Q_{11} &= E_1/1-\upsilon_{12}\upsilon_{21} \\ Q_{12} &= \upsilon_{12}\, E_2/1-\upsilon_{12}\upsilon_{21} = \upsilon_{21}E_1/1-\upsilon_{12}\upsilon_{21} \\ Q_{22} &= E_2/1-\upsilon_{12}\upsilon_{21} \\ Q_{66} &= G_{12} \end{aligned} \tag{2}$$

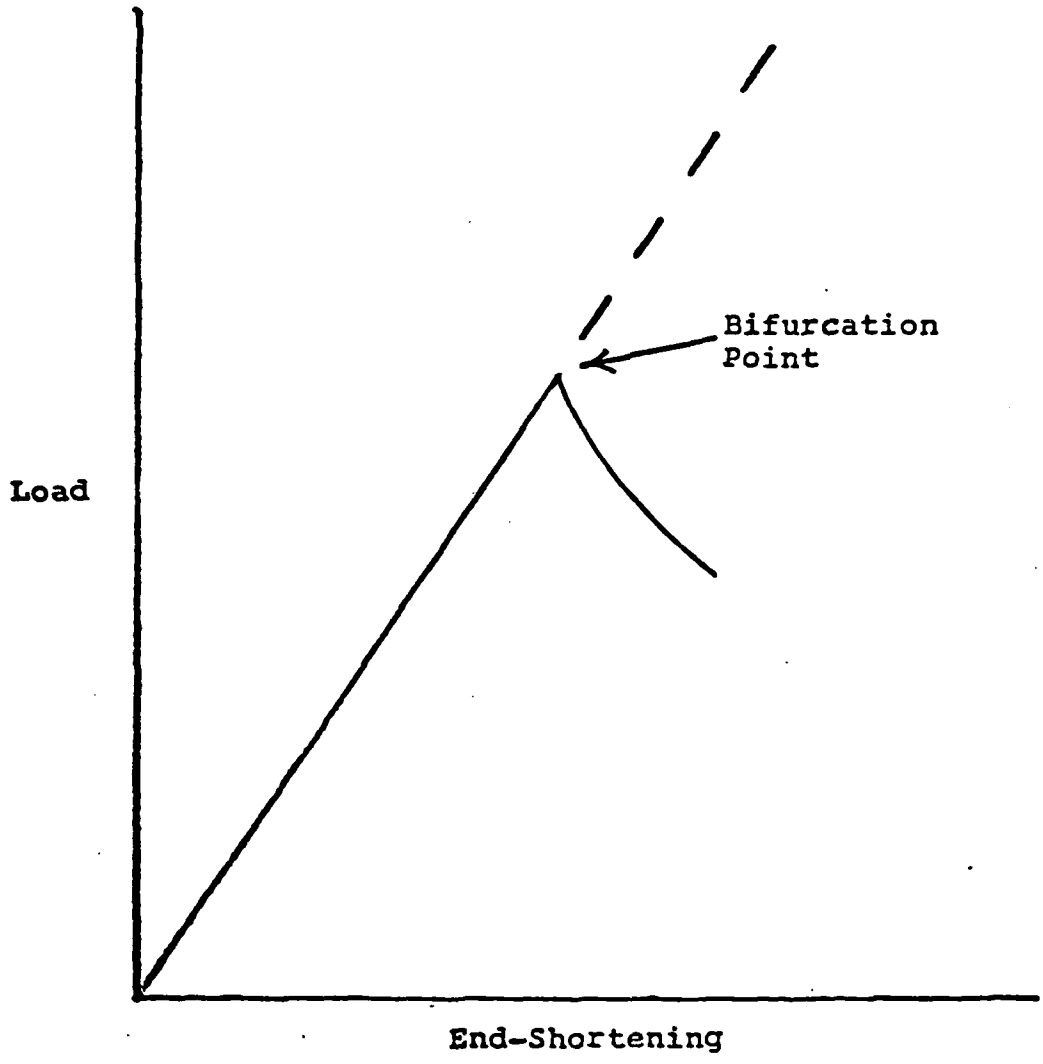

Load-Deflection Curve

Figure 2

II. Theory

Bifurcation Buckling

During the past 25 years, the study of the stability of shells has become one of the most investigated structural problems [14]. As a consequence of these investigations, many theories of buckling are available, but none has yet become universally accepted. Yet, the results of these studies have contributed to the understanding of many aspects of shell stability.

Buchert [15] defines buckling as "collapse of a structure under stress or loads that are less than those causing material failures." With this definition, the term buckling is used synonymously with the bifurcation point throughout this thesis. The concept of buckling, and the bifurcation point, can best be explained with a plot of load versus end-shortening of the panel [14]. Fig. 2 is a typical plot of load versus end-shortening for a thin shell.

For small loads and deflections, the curve is a straight line representing the equilibrium state of the shell. As the load is increased, the bifurcation point is reached. At the bifurcation point, there are two theoretically possible paths. The upper path implies buckling is prevented and the usual load-stress-strain-deflection relations hold true. However, this state

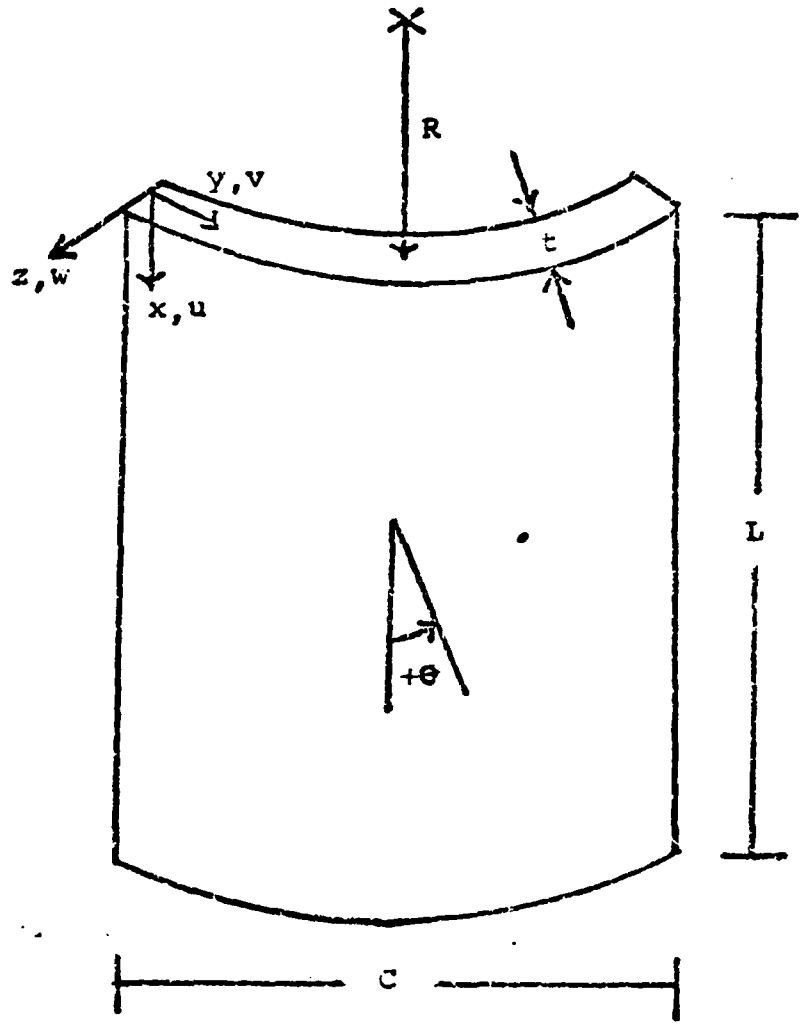

x,y,z = structural coordinates

u,v,w = displacements

t = thickness

R = radius of curvature

C = chord

L = length

θ = ply orientation

Panel Notation

Figure 1

$[0/90]_{2s}$. Three different size delaminations were included; 0 inch (no delamination), 2 inch circular, and 4 inch circular. The panels were manufactured with 8-ply graphite-epoxy with all delaminations placed at the midsurface and located at the geometric center of the panel. A total of 24 panels were tested which represents a duplication of each aspect ratio, ply orientation, and delamination size.

The material properties were determined experimentally for a given ply:

$$E_1 = 20.97 \times 10^6 \text{ psi}$$

$$E_2 = 1.53 \times 10^6 \text{ psi}$$

$$G_{12} = .815 \times 10^6 \text{ psi}$$

$$\upsilon_{12} = 0.300$$

The panel boundary conditions incorporated in the experimental test device provided a clamped top edge ($u = v = w = w_{,x} = 0$), clamped bottom edge (u = free, $v = w = w_{,x} = 0$); and simply supported on the vertical sides. See Fig. 1 for a description of panel dimensions and displacements.

work of Yin and Fei [13] refined the analysis to include a circular delamination in a thin, circular plate. Their results indicate a panel under pure compression will only buckle, while a panel loaded under both compression and bending will experience buckling, snap-through (separation of the delaminated layer from the main body of the plate), and catastrophic failure if the load is sufficient to attain the critical value for growth of the delamination.

Purpose

The purpose of this thesis is to experimentally determine the buckling loads of cylindrical composite panels with circular delaminations positioned in such a fashion that the shell skin and delamination buckle together. Limiting values on the experimental loads are determined from the linear bifurcation load calculated by the STAGSC-1 Finite Element Computer Code. Three major variables are included in the study: ply orientation, aspect ratio, and delamination size. The results are used to further the understanding of composite buckling behavior and increase the data base available to users of composite materials.

Scope

The experimental panels consisted of two different aspect ratios, 1(12 X 12) and 1 1/2 (12 X 8), and two different ply orientations, $[0/-45/+45/90]_S$ and

compared to theoretical values. These investigations continued [4, 5] as both experimental and analytical techniques were refined, resulting in a broader, more reliable data base that provides comprehensive set of buckling load data for a wide range of panel aspect ratios (length/chord) and ply orientations. To continue the understanding of the buckling problem, researchers have begun examining the effects of different variables on the buckling problem. Boundary conditions are one variable that has a substantial effect on the buckling load of the panel [6, 7]. These investigations indicated that the buckling load increases as degrees of freedom are restrained at the boundary condition, resulting in a stiffer panel. Another variable considered in recent studies is panel imperfections [8]. These imperfections range from eccentricities caused by the manufacturing process or test fixture installation to cutouts that remove a percentage of the panel's area [9].

Recently numerous articles have dealt with the effects of a delamination on an axially loaded laminated plate. Analytical approaches to the problem [10, 11, 12] developed techniques to determine a flat panel's axial load capacity for a variety of boundary conditions, delamination lengths, and plate and delamination thicknesses. However, these techniques were limited to a one-dimensional, across-the-width, delamination. The

THE EFECT OF CENTER DELAMINATION ON THE INSTABILITY OF COMPOSITE CYLINDRICAL PANELS

I. Introduction

Background

The benefit of composite material's high strength to weight ratio make it an excellent material for use in modern aircraft structures. The USAF's commitment to the use of composite aircraft structural parts has resulted in the Air Force Aeronautical Systems Division recently awarding a contract to McDonnell Douglas Corp. for the development of a computerized system to control the autoclave curing process [1]. Also, NASA is currently engaged in developing and demonstrating the efficient use of composites in airframe structures on large transport aircraft [2]. This widespread use of composite materials has accounted for an increase in the amount of analytical and experimental research on the behavior of composites. However, one area of research still in its early stages is the effect of a delamination or debonding on the overall stability of a laminated panel.

Initial development of procedures to experimentally determine the buckling load of curved composite panels was done by Wilkens [3], who also presented a percent knockdown factor, $\left((1-\frac{\text{experimental buckling load}}{\text{theoretical buckling load}}) \times 100\right)$, to show the decrease in experimental buckling loads as

Further simplifications to the integrations are possible by recalling the strains and curvatures in Equations (13) and (14) are mid-surface values and not functions of z.

Hence, they too can be removed form the integration and the moment and force equations become:

$$\begin{Bmatrix} N_x \\ N_y \\ N_{xy} \end{Bmatrix} = \begin{bmatrix} A_{11} & A_{12} & A_{16} \\ A_{12} & A_{22} & A_{26} \\ A_{16} & A_{26} & A_{66} \end{bmatrix} \begin{Bmatrix} \epsilon_x^0 \\ \epsilon_y^0 \\ \gamma_{xy}^0 \end{Bmatrix} + \begin{bmatrix} B_{11} & B_{12} & B_{16} \\ B_{12} & B_{22} & B_{26} \\ B_{16} & B_{26} & B_{66} \end{bmatrix} \begin{Bmatrix} K_x \\ K_y \\ K_{xy} \end{Bmatrix} \quad (15)$$

and

$$\begin{Bmatrix} M_x \\ M_y \\ M_{xy} \end{Bmatrix} = \begin{bmatrix} B_{11} & B_{12} & B_{16} \\ B_{12} & B_{22} & B_{26} \\ B_{16} & B_{26} & B_{66} \end{bmatrix} \begin{Bmatrix} \epsilon_x^0 \\ \epsilon_x^0 \\ \gamma_{xy}^0 \end{Bmatrix} + \begin{bmatrix} D_{11} & D_{12} & D_{16} \\ D_{12} & D_{22} & D_{26} \\ D_{16} & D_{26} & D_{66} \end{bmatrix} \begin{Bmatrix} K_x \\ K_y \\ K_{xy} \end{Bmatrix} \quad (16)$$

or

$$\begin{Bmatrix} N_x \\ N_y \\ N_{xy} \\ M_x \\ M_y \\ M_{xy} \end{Bmatrix} = \begin{bmatrix} [A] & [B] \\ [B] & [D] \end{bmatrix} \begin{Bmatrix} \epsilon_x^0 \\ \epsilon_y^0 \\ \gamma_{xy}^0 \\ K_x \\ K_y \\ K_{xy} \end{Bmatrix} \quad (17)$$

where A_{ij} are the extensional stiffnesses, B_{ij} are the coupling stiffnesses, and D_{ij} are the bending stiffnesses.

$$A_{ij} = \sum_{k=1}^{N} (\bar{Q}_{ij})_k \ (z_k - z_{k-1})$$

$$B_{ij} = \frac{1}{2} \sum_{k=1}^{N} (\bar{Q}_{ij})_k \ (z^2_k - z^2_{k-1}) \qquad (18)$$

$$D_{ij} = \frac{1}{3} \sum_{k=1}^{N} (\bar{Q}_{ij})_k \ (z^3_k - z^3_{k-1})$$

Delamination Panel Buckling/Postbuckling States

There are three distinct states to the buckling/ postbuckling problem of panels containing delaminations defined by Fei and Yin [13]: bifurcation, snap-through, and catastrophic failure. The bifurcation phenomena results from the panel being subjected to pure compression and the delaminated layer maintains full contact with the main body of the plate. With the introduction of bending and the proper ratio of bending moments to the compressive load, snap-through of the delaminated region will occur. Snap-through is defined as separation of the delaminated layer from the main body of the plate. A continued increase in the load past the snap-through states results in an increasing energy release rate. When the energy release rate reaches the critical value for growth of the delamination, the delamination will grow and catastrophic failure will occur.

In their analysis of the postbuckling problem, Fei and Yin [13] developed three non-dimensionalized expressions for bending strain versus membrane strain, delamination radius and energy release rate. The expressions considered a homogeneous, isotropic, circular plate with a centrally located circular delamination subjected to axis symmetric edge compression and bending moment along its boundary. The three relationships are:

$$\rho = \upsilon h/2\epsilon$$

- bending strain versus membrane strain (19)

$$\tilde{a} = [12(1-\upsilon^2)\epsilon\ ]^{1/2}\ a/h$$

- non-dimensionalized delamination radius (20)

$$\tilde{G}\tilde{a}^4 = \left|12(1-\upsilon^2)\right|^2\ G^*a^4/Eh^5$$

- non-dimensionalized energy-release rate (21)

where:

μ - curvature to the plate middle surface

h - depth, measured from top surface, of delamination

ϵ - compressive membrane strain in delaminated layer

υ - Poisson's Ratio

a - delamination radius

G^* - material fracture toughness

E - Young's Modulus

Their results, presented in table and graph form, relate the three non-dimensionalized terms to determine which buckling/postbuckling state the plate will experience.

This thesis is concerned with determining the initial buckling load of a panel with a delamination located at the midsurface. The results of Fei and Yin are used to confirm that due to the delamination being located at the midsurface and the small ratio of bending strain to membrane strain, snap-through will not occur on any of the panels. Sample calculations of the non-dimensionalized terms are presented in Appendix C.

STAGSC-1 Theory

STAGSC-1 (Structural Analysis of General Shells) is an energy based, finite element computer program. The code, developed by Lockheed Palo Alto Research Laboratory, was developed to analyze shell structures under various loadings and boundary conditions. The eigenvalue solutions used in this thesis were obtained from a linear analysis utilizing the QUAF 411 element. The grid size for each panel was 1 inch by 1 inch. For further information on STAGSC-1 Linear Analysis and grid modeling, the reader is referred to references [5] and [18].

III. Manufacturing and Experimental Procedures

Panel Manufacturing

The panels used in the compression tests were constructed from Hercules AS4/3502 Graphite/Epoxy 12 inch tape. An initial set of two flat panels, one $[0/90]_{2S}$ lay-up and one $[0/-45/+45/90]_S$ lay-up, were constructed to determine a suitable material to cause a delamination. Six material combinations were tested in each of the panels: mylar (t = 1 mil), mylar with release, backing paper (t = 5 mil), backing paper with release, non-porous teflon (t = 3 mil), and nylon peel ply (t = 3 mil). The release used was RAM 225 and it provided a further safeguard to prevent bonding. After the curing cycles, each panel was examined by a C-Scan to confirm delamination had occurred and also to insure the delaminations had not moved during the lay-up and curing process. The C-Scan results indicated all six materials had caused delaminations and none of the materials shifted or moved during the manufacturing process. As a further check, one panel was cut length-wise through the delaminations (Fig. 6) and notches were cut from each delaminated section. Again, both sides of the panel fell apart at the delamination indicating a complete lack of bonding around each material. The material chosen for the curved panel delaminations was the mylar with release

because it had the smallest thickness of the four materials.

All curved panels were hand laid on a curved plate with the required 12 inch radius of curvature. Mylar templates (Fig. 7) were cut for each mold in order to place the delamination material at the proper location (Fig. 8). Following the lay-up, the panels were transferred to the steel molds (Fig. 9). In the molds the panels were prepared for the autoclave and sealed in a nylon vacuum bag (Fig. 10). The entire lay-up was cured according to the following cure cycle:

(1) Apply full vacuum (2.42 psia minimum) to sealed lay-up

(2) Heat to 270° F in 45±5 minutes

(3) Hold 270° and full vacuum for 15 minutes

(4) Pressurize autoclave to 85 psi

(5) Hold at 270° and 85 psi for 45 minutes

(6) Heat to 350° F

(7) Hold at 350° F and 85 psi for 15 minutes

(8) Vent lay-up bag vacuum

(9) Hold at 350° F and 85 psi for 105 minutes

(10) Cool to below 150° F in 60 minutes maintaining 85 psi

(11) When below 150° F, vent pressure

Mylar with Release

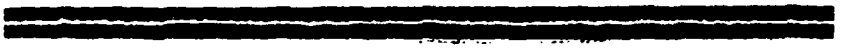

Peel Ply

Midsurface Delaminations

Figure 6

Template to Position Delamination

Figure 7

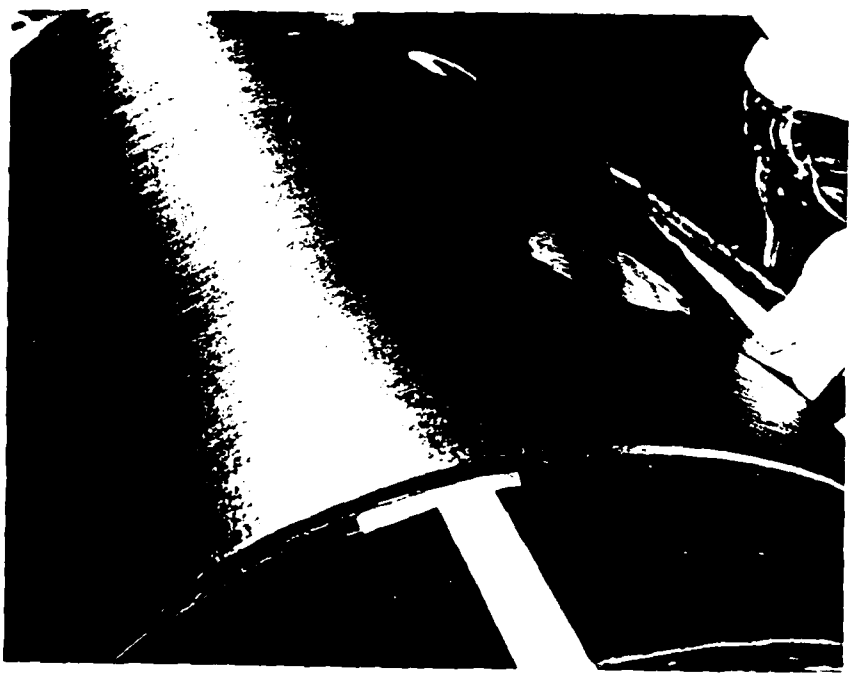

Midsurface Circular Delaminations

Figure 8

After curing, the panels were checked by C-Scan techniques to insure no voids were present. In addition, a hand-held ultrasonic test devise was used on each panel to accurately mark the delamination location, Fig. 11. These panel markings were permanent in order to use as a reference comparison after the panel buckling phase of the experiment was carried out.

Each cured lay-up was cut into four panels of the desired experimental size. The test panels were cut on a specially jigged radial arm saw with a diamond tipped blade. After each panel was cut, a series of 8 length, 4 chord, and 12 thickness measurements were taken . The thickness measurements showed the panel variation was less than 1.0 percent for any panel. The length dimensions are very critical to insure an even load distribution throughout the test. From this thesis and previous experiments conducted with the compression [5, 9], it was determined that variations greater than .01 inch on a 12 inch chord and .007 inch on an 8 inch chord were unacceptable. All chord measurements were acceptable since a quarter inch gap was available on the vertical side supports.

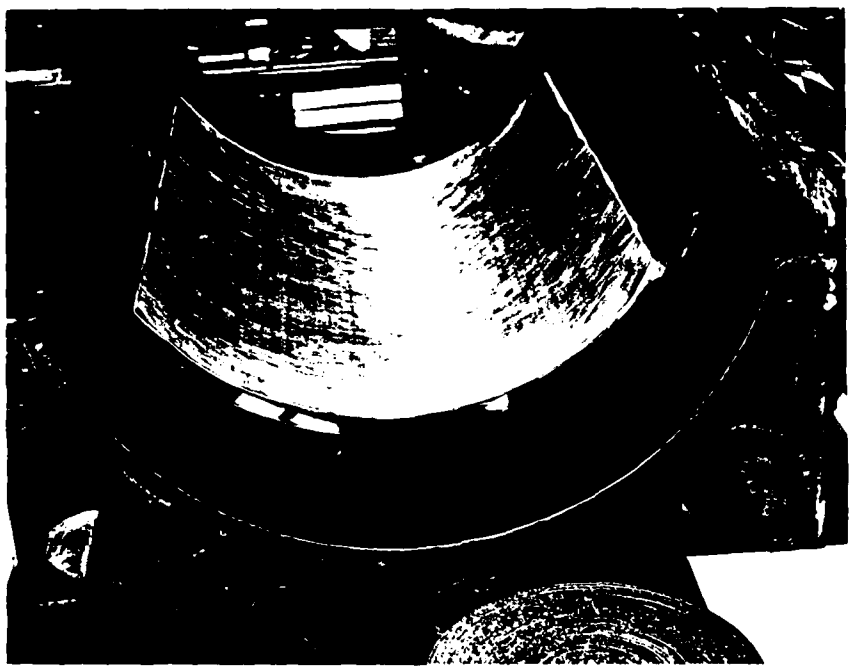

Panels Positioned in Mold

Figure 9

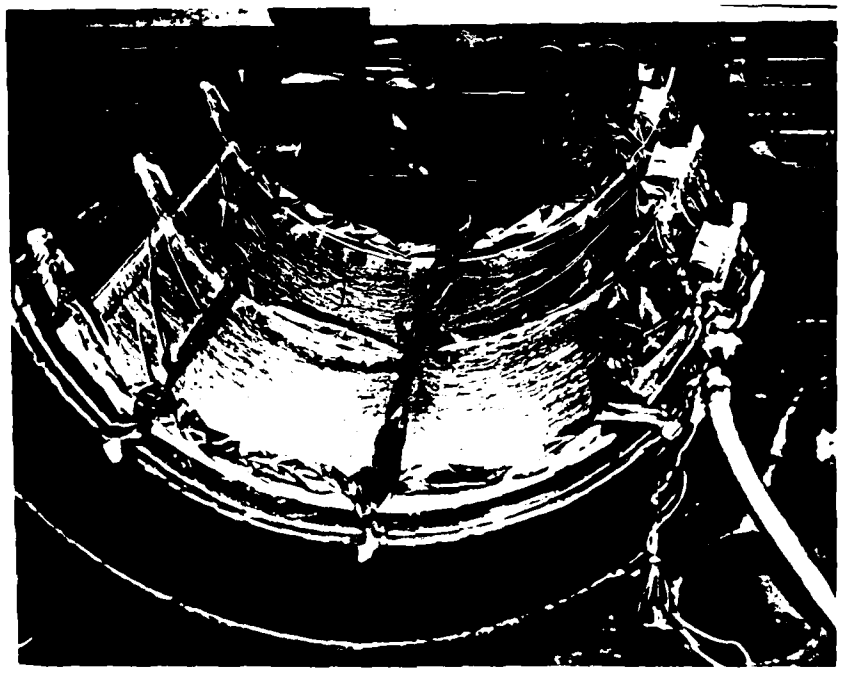

Panels/Mold Prepared for Autoclave

Figure 10

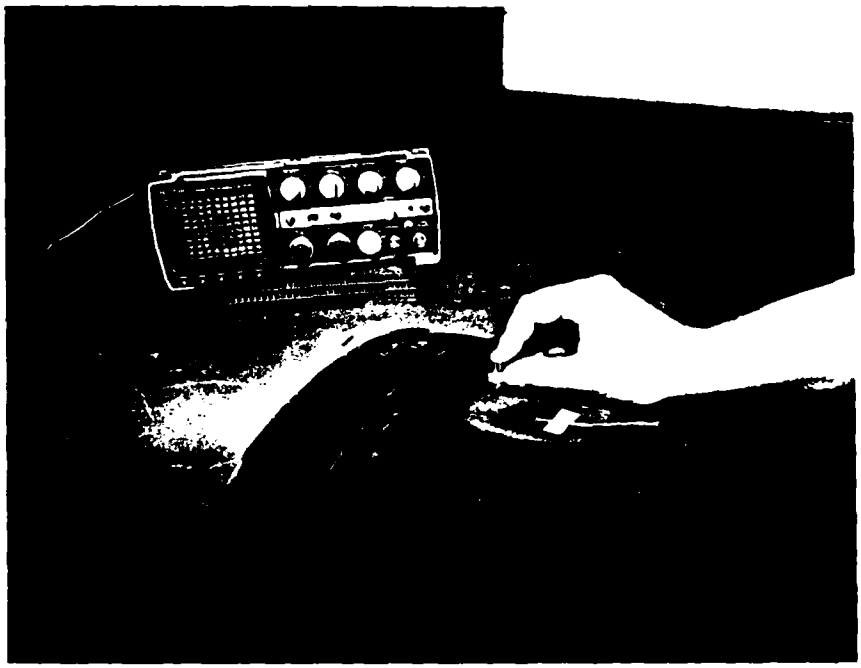

Hand-held Ultrasonic Equipment

Figure 11

Experimental Set-Up

The test device used in this thesis required a modification of a current compression testing system. This device has a 30K lb capacity and was modified with fixtures to hold the curved panels. Boundary conditions assumed to be provided by the test set-up are a clamped top edge ($u = v = w = w_{,x} = 0$), clamped bottom edge (u = free, $v = w = w_{,x} = 0$), and simple supports along both vertical sides ($u = v = w_{,y}$ = free, $w = 0$).

Both top and bottom plates of the test fixture are bolted directly to the cross heads of the compression machine. The load is applied to the bottom cross head by a hydraulic ram. Clamped boundary conditions are obtained by a set of blocks forced against the top and bottom edges with a series of screws. The screws are tightened with a screwdriver to eliminate any panel movement. Center lines are marked on both top and bottom test fixtures to insure the panel is properly centered.

Simply supported side boundary conditions are provided by two bars clamped in each side support. The edges of the bars are thin knife like edges that allow the panel to rotate in the $w_{,y}$ direction. Figure 12 shows the side supports with the bars and plates used to clamp the bars in the side supports. When inserting the panel, a series of five set screws are tightened on each side of the support. These set screws are finger tightened until the knife edges just contact the panel.

In all tests the top and bottom of the panel were clamped first, then the simple supports were installed and the set screws finger tightened. A 1/4 inch space occurred between the knife edges and the bottom supports to allow the panel to compress. By adjusting the knife edges, this 1/4 gap is placed at the bottom to achieve buckling symmetry [5]. Fig. 13 shows the complete experimental set up with panel installed.

When conducting buckling experiments, two problems have constantly plagued investigators, those of proper load introduction [19], and the effects of boundary conditions changing during the experiment [14]. Both of these problems were encountered during the experiments for this thesis. However, by carefully following the above procedure for panel installation, the effects of these two problems were minimized.

Instrumentation consisted of four axial strain gages and an LVDT (Linear Variable Differential Transducer). The LVDT, visible on the right side of the test fixture in Fig. 14, was mounted on the cross heads to measure end-shortening of the panel. Two of the strain gages were mounted two inches from the bottom of the panel and three inches from the panel center line (two inches from panel center line on panels with an eight inch circumference) to insure uniform loading. Two additional gages were mounted back-to-back at the geometric center of the

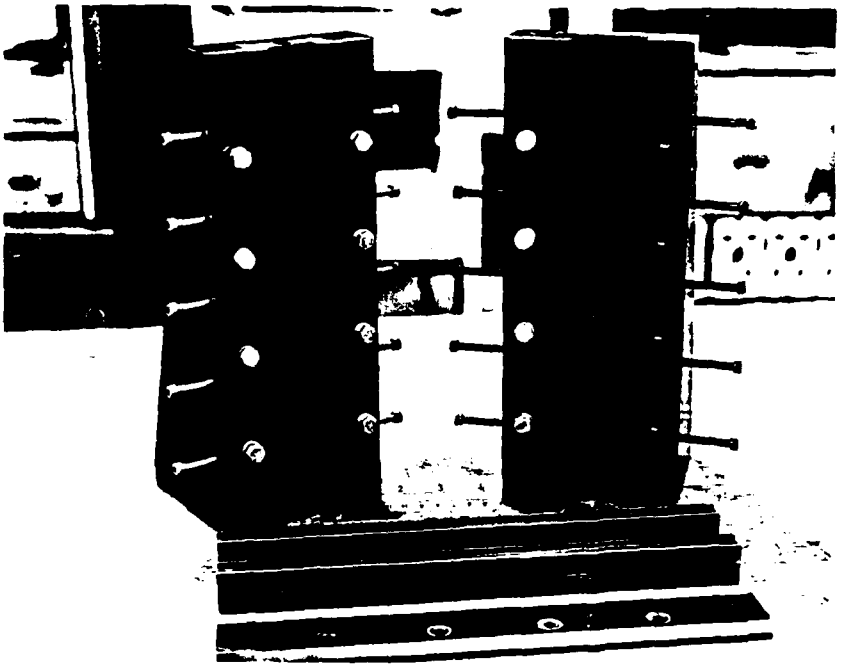

Vertical Side Supports

Figure 12

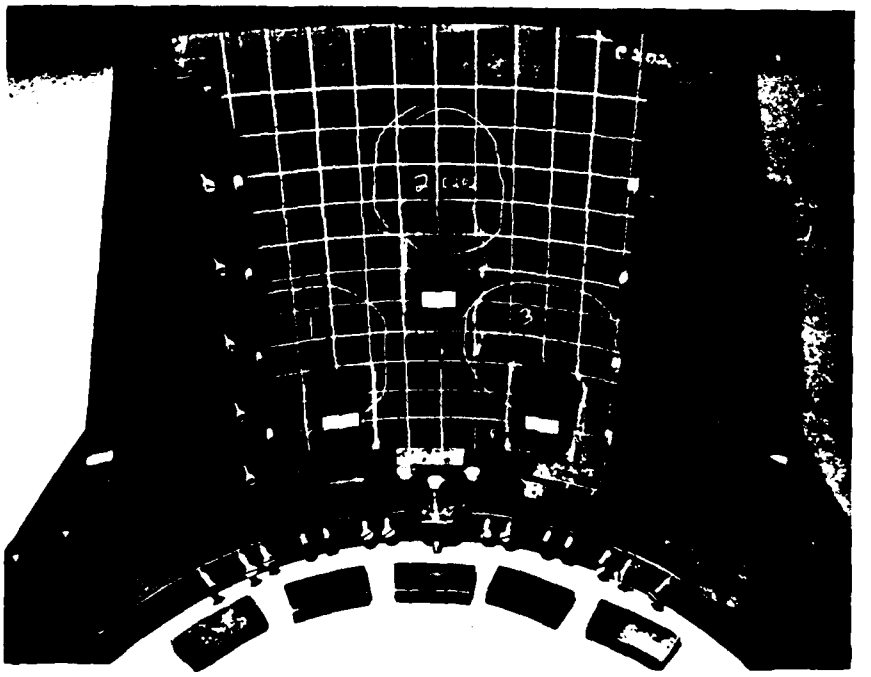

Panel Mounted in Support Fixture

Figure 13

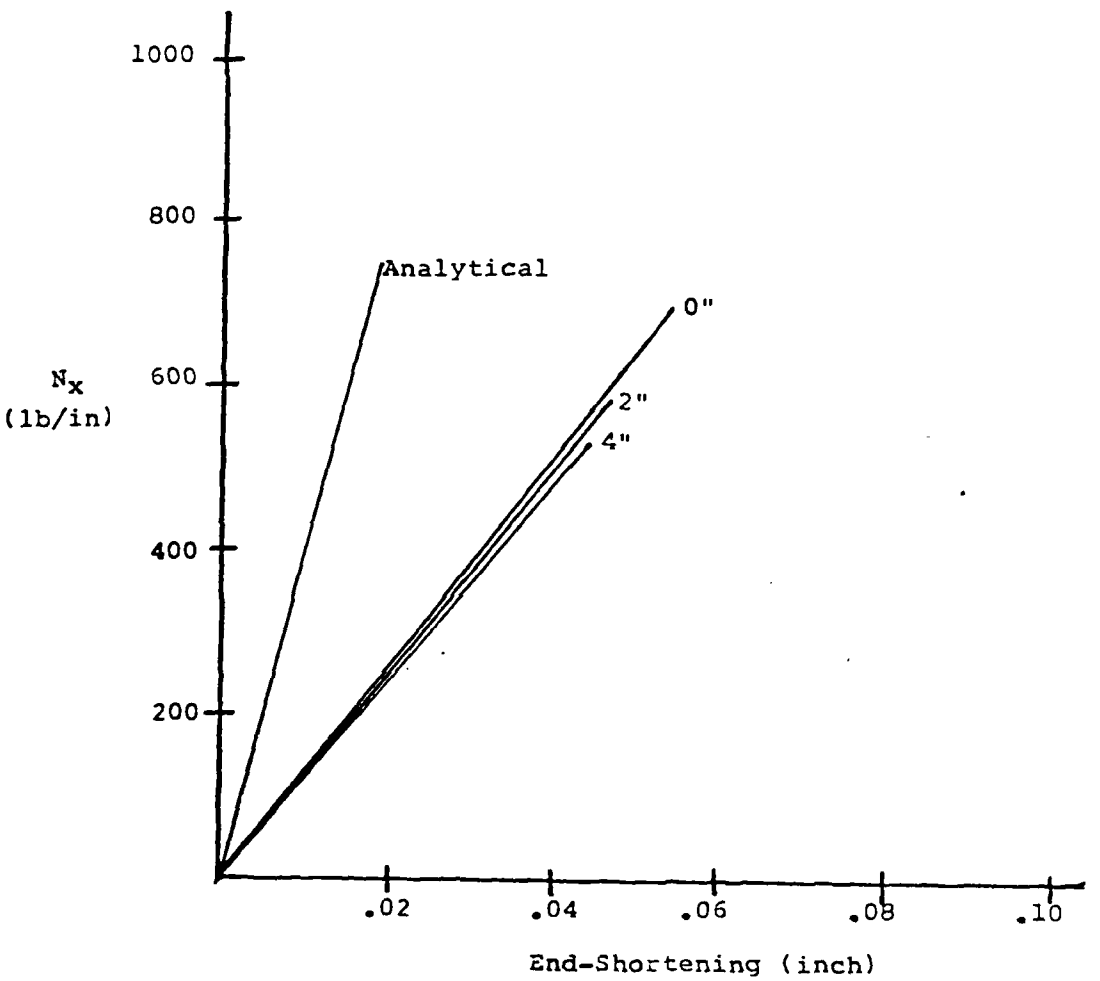

Analytical/Experimental Results

$[0/90]_{2s}$ AR = 1 1/2

Figure 19

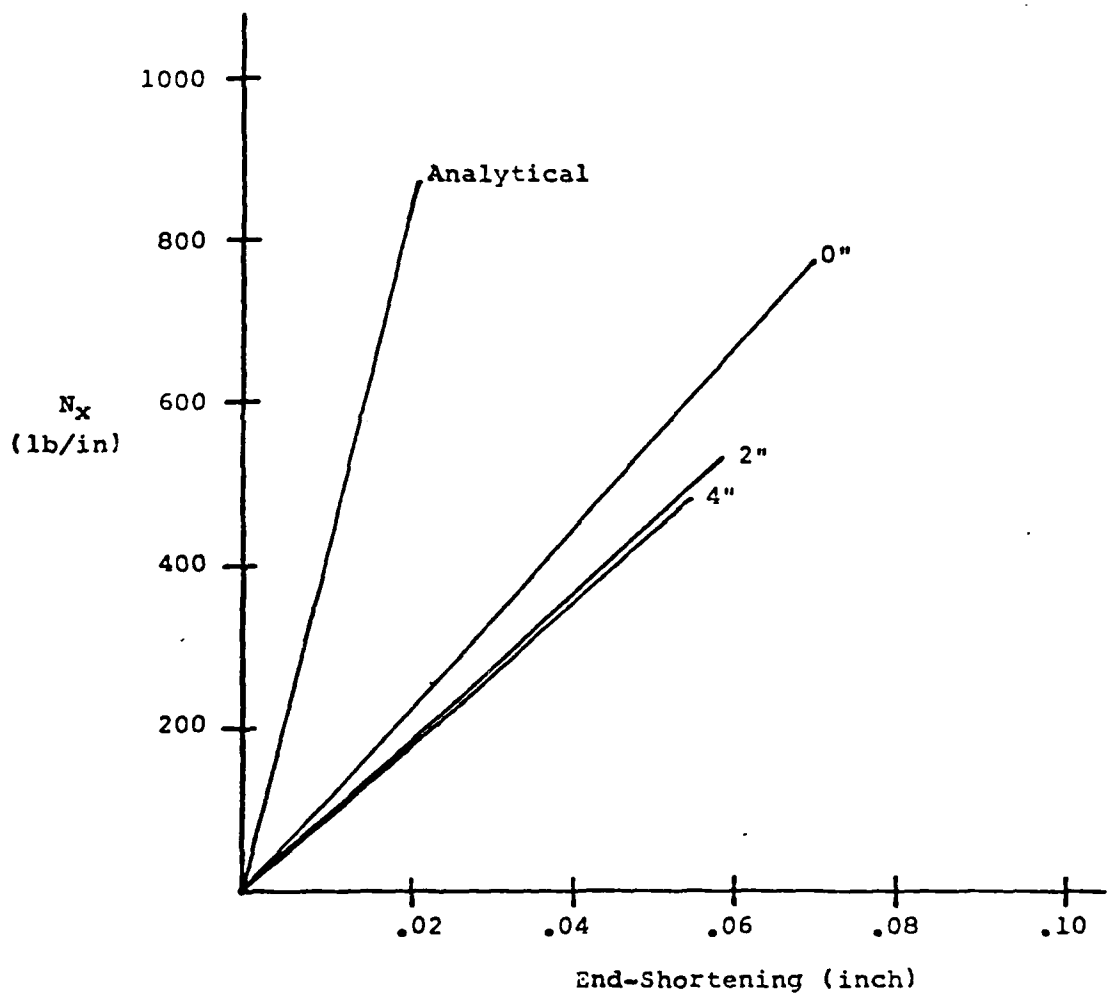

Analytical/Experimental Results

$[0/-45/+45/90]_S$ AR =1 1/2

Figure 18

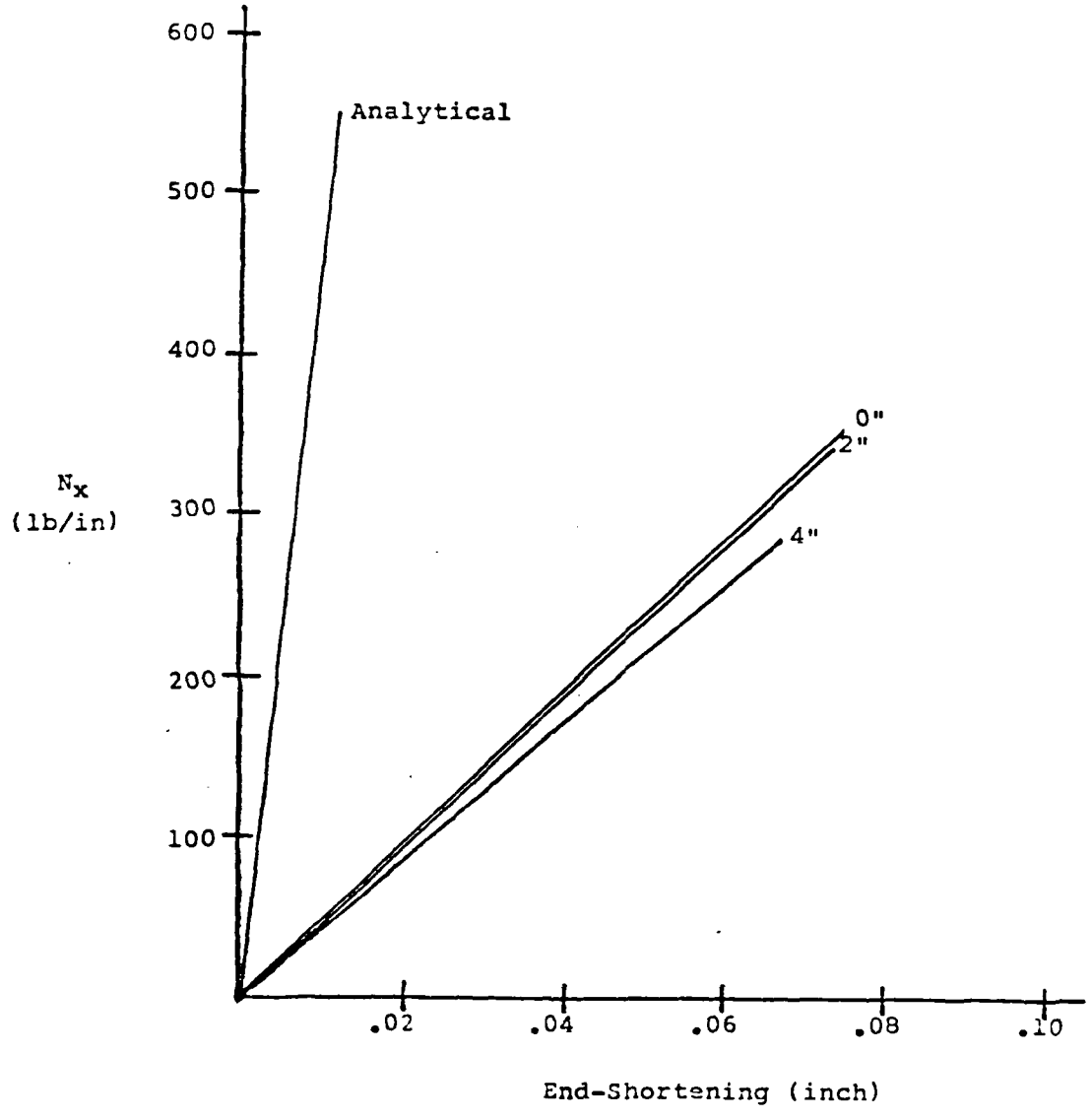

Analytical/Experiment Results

$[0/90]_{2s}$ AR = 1

Figure 17

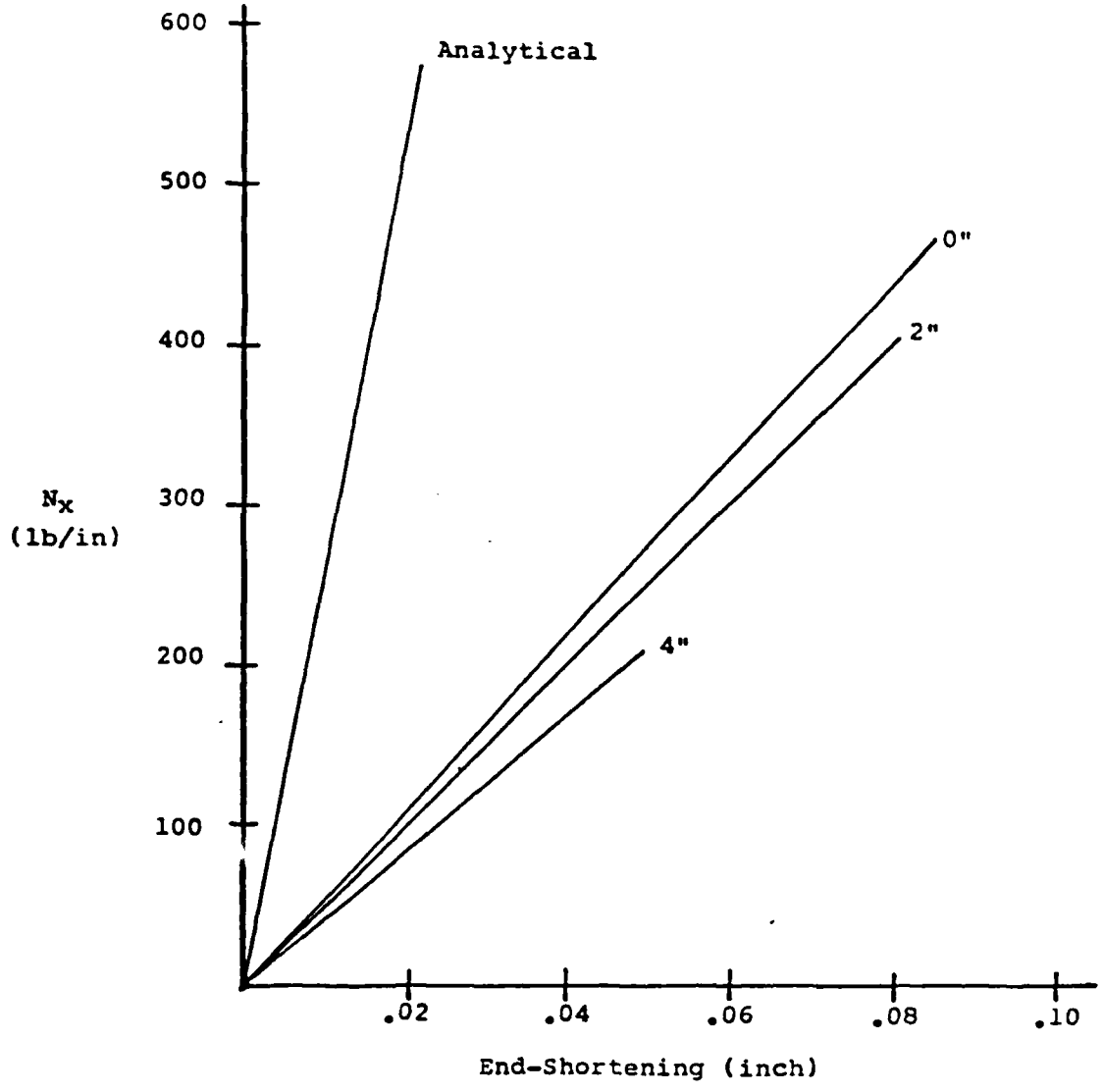

Analytical/Experimental Results

$[0/-45/+45/90]_S$ AR = 1

Figure 16

confirmed by examining the experimental results. The reader will recall the two strain gages placed equidistant from the center line to determine whether the load was applied symmetrically. An unsymmetric load application resulted in one gage showing more compressive strain than the other gage. Since the side showing more strain also was taking more of the load, the first buckle occurred on this side of the panel. By further increasing the load, the other side of the panel began taking the load and would then buckle. This phenomena was confirmed by comparing buckling/postbuckling, strain gage output, and buckling patterns. However, analyzing the varying boundary conditions and the postbuckling problem are beyond the scope of this thesis.

Plots of load versus end-shortening for the analytical and experimental values are shown in Figures 16-19 through the first buckle only. These four figures indicate the reduction in stiffness for each panel as the delamination size increases. Also, when comparing panels with equal aspect ratios and different ply orientations, it is shown the $[0/-45/+45/90]_S$ panels have a greater reduction in stiffness as delamination size increases when compared to the $[0/90]_{2S}$ panels.

Panel ID	Analytical Bifurcation Load (lb)/N_x (lb/in)	Experimental Result Load(lb)/N_x(lb/in)	Knockdown Factor % (1)	Knockdown Factor % (2)
Q20	6888.0/574.0	5574.6/464.6	19.1	----
Q22	--	4845.4/403.8	--	13.1
Q24	--	2527.1/210.6	--	54.7
C20	6602.4/550.2	4275.0/356.8	35.2	--
C22	--	4181.9/348.5	--	2.2
C24	--	3453.9/287.8	--	19.2
Q80	7010.4/876.3	6246.9/780.9	10.9	--
Q82	--	4135.6/517.0	--	33.8
Q84	--	3976.7/497.0	--	36.3
C80	6065.6/758.2	5607.7/701.0	7.5	--
C82	--	4717.8/589.7	--	15.9
C84	--	4261.6/532.7	--	24.0

$$1) = \left(1 - \frac{\text{Experimental Result}}{\text{Analytical Bifurcation}}\right) \times 100$$

$$2) = \left(1 - \frac{\text{Experimental Result}}{\text{Experimental Result (No delamination)}}\right) \times 100$$

Analytical/Experimental Results

Table II

Panel ID	Buckling Load (lb)	End-Shortening (in)
Q201	5574.6	.0842
Q221	5027.4	.0833
Q222	4663.3	.0801
Q242	2527.1	.0493
C201	4275.0	.0732
C221	4181.9	.0719
C242	3453.9	.0678
Q802	6246.9	.0700
Q822	4135.6	.0586
Q841	4157.0	.0529
Q842	3796.3	.0555
C802	5607.7	.0528
C821	4825.5	.0480
C822	4610.0	.0456
C841	4038.0	.0398
C842	4485.2	.0424

Experimental Results

Table I

providing the desired boundary conditions. The frequent unsymmetric buckling patterns and the postbuckling strength exhibited by the panels led to the assumption that the vertical side supports were providing more restraints than the desired simple support. To verify this assumption, STAGSC-1 modeling was accomplished by varying the vertical side boundary conditions. The results of numerous previous buckling experiments have confirmed that an analytical buckling load with no panel imperfections is higher than an experimentally determined load for the same panel. Therefore, the initial modeling consisted of simply supported ($u = v = w_{,y}$ = free, $w = 0$) boundary conditions and then eliminating certain degrees of freedom. From the simple support conditions, first u was fixed and then both u and v fixed. To achieve an analytical bifurcation load higher than the experimental value, it was necessary to have both u and v fixed along the vertical sides. These are the analytical values presented in Table II. In addition to increasing the initial buckling load, a stiffer panel will exhibit greater postbuckling strength as was evidenced in these experimental tests. To properly analyze this phenomena, one would have to vary the boundary conditions as the load is applied and the panel becomes progressively restrained. To further complicate the problem, the restraints are not applied symmetrically. This finding is

Table I shows the experimental results for the panels. The reader will notice that of the 24 manufactured panels, only 16 are included in the results. Of the remaining eight panels, seven were rejected due to exceeding the length dimension tolerance. These tolerances of .01 inch variation on panels with AR = 1 and .007 inch variation on panels with AR = 1 1/2 were reconfirmed after examining the experimental output. Exceeding these tolerances prohibited an even load distribution through the panel, verified by the unacceptable differences between the two strain gages mounted to monitor load introduction and what appeared to be shear-induced buckling patterns.

Analytical/Experimental Comparison

To this author's knowledge, there are no analytical expressions or computer coded models that will solve the problem of a curved composite panel with a delamination located at the midsurface. Therefore, in order to establish limits on the experimental results, the STAGSC-1 code was used to model the panels with no delamination and establish an upper bound on the buckling loads. These analytical results and final experimental values are presented in Table II.

It became apparent during the initial stages of the compression testing that the test fixture was not

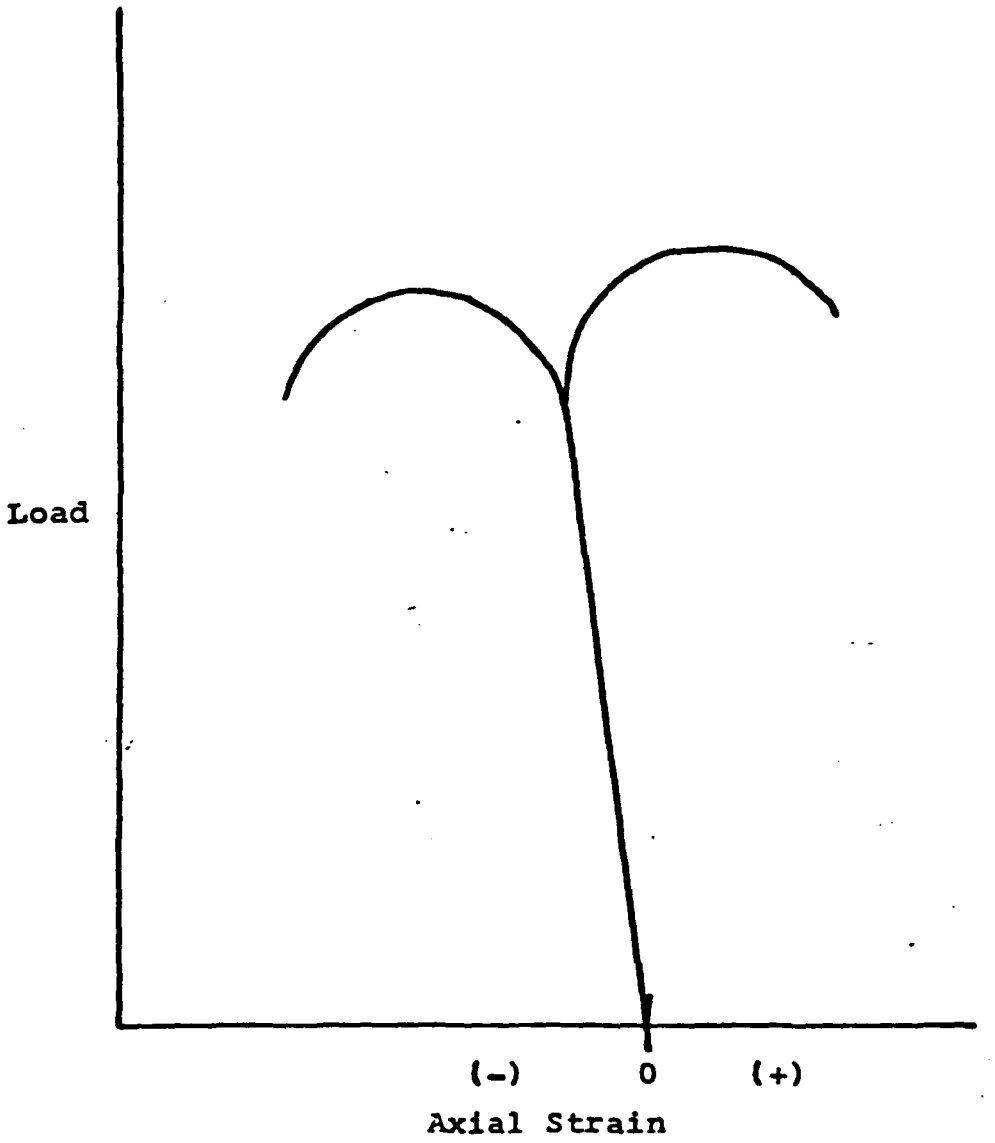

Strain Reversal

Figure 15

versus panel end-shortening and load versus back-to-back strain gages are used to determine the panels' buckling load. The third plot was load versus the two remaining strain gages and is used to insure the load is evenly applied to the panel.

The use of a load versus deflection (or end-shortening) plot to determine buckling load was explained in reference to Fig. 2. Another technique to determine buckling loads is known as a strain reversal technique. This method is shown in Fig. 15 and requires the output of back-to-back strain gages. As the load is initially applied and begins to increase, both strain gages register the same amount of compression. The gages continue to read the same increase in strain until the panel buckles. At this point, the strains of the respective gages increase dramatically in both tension and compression indicating the physical presence of a buckle. One limitation to this technique is that it requires a prior knowledge of the panel's buckling pattern to insure the back-to-back gages are located at the initial buckle. The back-to-back gages on these panels were located at the geometric center of the panel, which is also the center of the delaminations. Since the initial buckle always occurred at the delamination, the strain reversal technique yielded the same buckling load as the load versus deflection plot.

IV. Results and Discussions

Panel Identification

The experimental panels are identified using the following system:

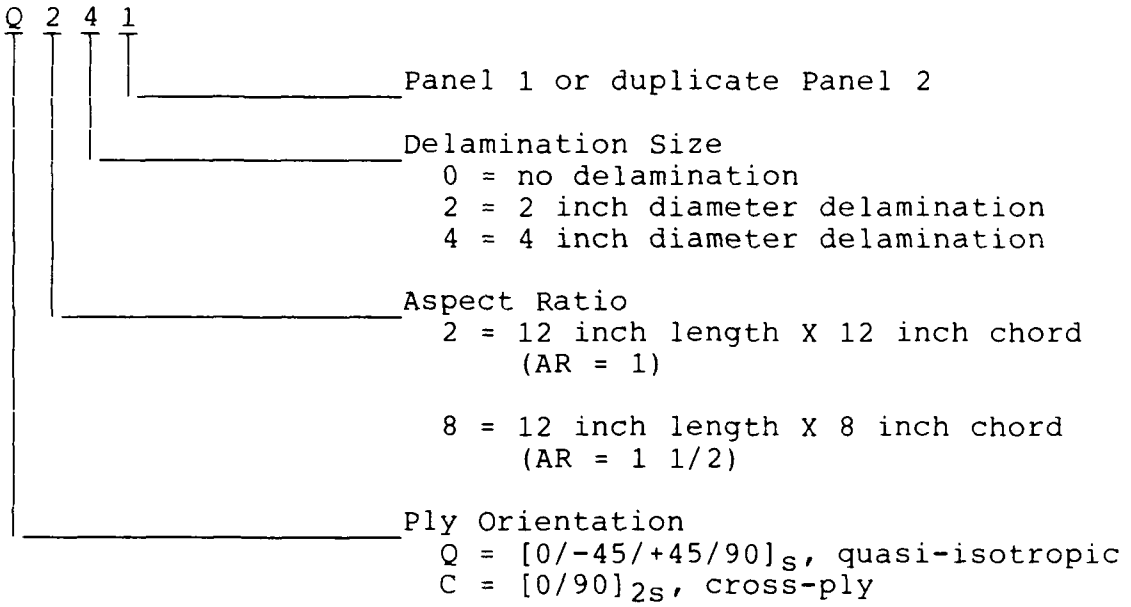

A three digit code is used to identify the average results of both duplicate panels. As an example, Q22 means the average values for panels Q221 and Q222.

Data Output

As stated previously, all data was stored on tape and printed out at a later time. The data from all instrumentation was referenced to a computer reference time and hence the output from any instrument channel could be compared. In addition to the printed data, three computer generated plots were available. Two plots, load

panel. This instrumentation provided the data to determine buckling loads by two techniques:

1. load versus end-shortening
2. strain reversal.

Test Procedure

Once the panel was installed, the LVDT and all strain gages were electronically zeroed. The load was applied at the rate of .055 inches per minute cross head speed and data was recorded ten times per second on a VAX 11/780 computer. Loading was held constant through the initial buckle and beyond in order to get a portion of the postbuckling curve. The buckling pattern was highlighted with a silver pencil and the pattern photographed. All data was stored in a real time mode and printed out later. Data from the load cell and the four strain gages was also displayed on a CRT during the tests to monitor load and load introduction to the panel.

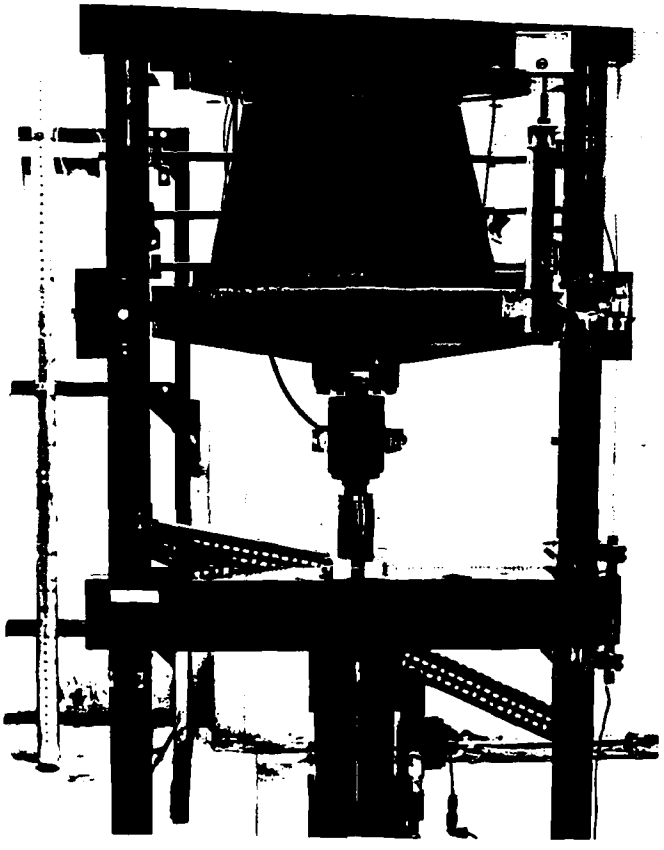

Complete Experimental Set-Up

Figure 14

Buckling Patterns

When installing the panel in the test fixture, it was found that by leaving the 1/4 inch of free space at the loading edge of the panel the buckling pattern would be symmetric [5]. The gap at the end where the load was applied allowed for a more even stress distribution. This symmetric buckling pattern can be seen in Fig. 20, a panel with no delamination. But, the buckling pattern differed when compared to panels that had delaminations. All panels with delaminations exhibited the initial buckle at the delamination location. However, the buckling patterns differed after the initial buckle appeared and the load was increased. Figures 21 and 22 represent two different post-buckling patterns. Fig. 21 is representative of a symmetric pattern where the initial buckle grew about the delamination and the pattern remained symmetric as two buckles appeared in the lower corners. In contrast, Fig. 22 shows a buckling pattern that grew from the initial buckle to a shear-type buckling pattern indicating a variable change in the boundary conditions on the vertical supports.

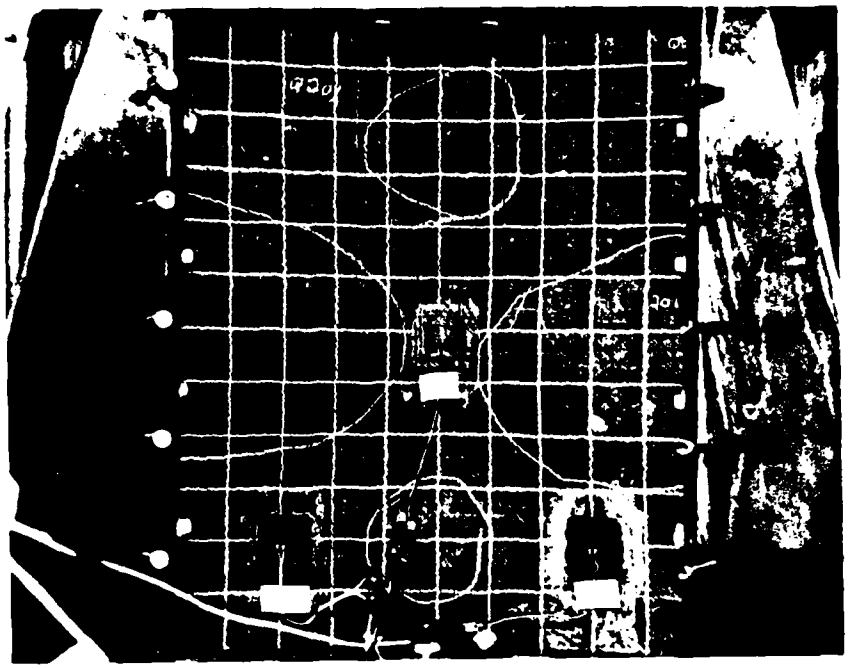

Q201 Buckling Pattern

Figure 20

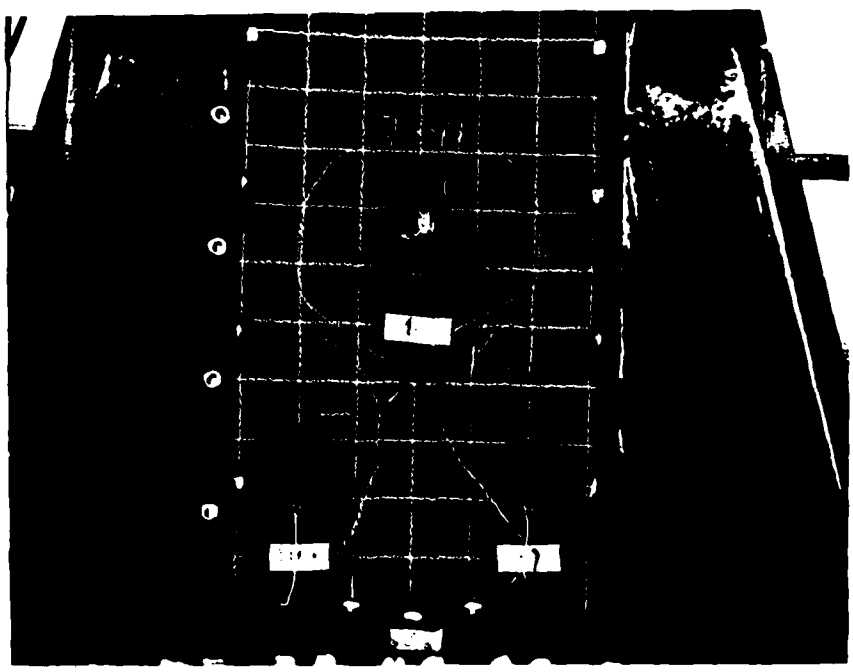

Q841 Buckling Pattern

Figure 21

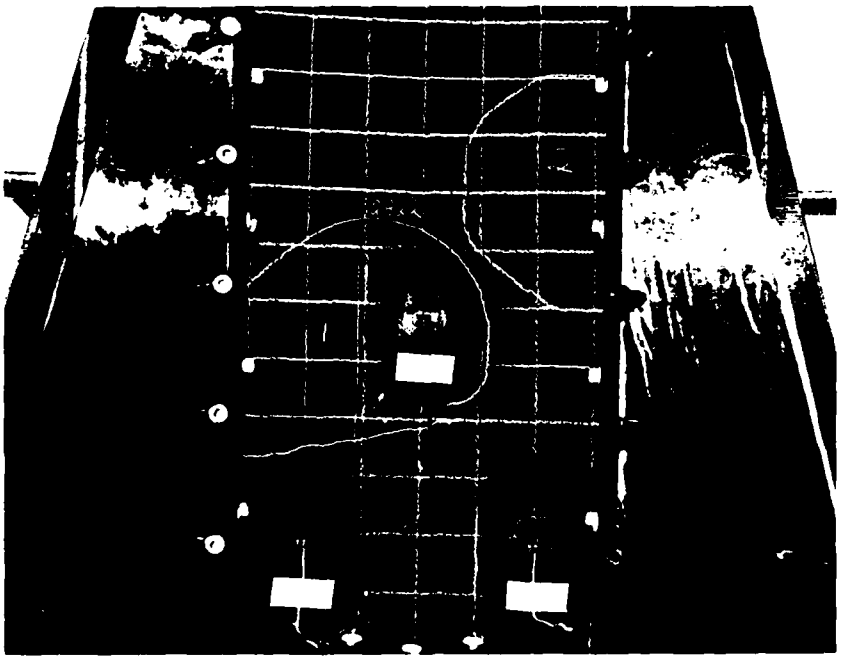

Q822 Buckling Pattern

Figure 22

Postbuckling Panel Inspection

The reader will recall the purpose of this thesis is to experimentally determine the buckling load of a delaminated panel where the delaminated layer maintains full contact with the panel. Visual observation of the buckling pattern for each test confirmed snap-through did not occur on any panel. To insure no delamination growth or any other panel damage occurred during the buckling, two techniques were employed. First, each panel was scanned using the same hand-held ultrasonic transducer (Fig. 11) used to locate the delamination after the panels were manufactured. Since each delamination had been permanently marked, it was a simple procedure to check for any delamination growth. By moving the transducer across the delamination, the edges were located and found to exactly coincide with the previous delamination markings for all panels. Thus, it was verified, no delamination growth occurred for any panels.

The second method involved the use of x-rays to check for any matrix cracking. This technique required the introduction of a penetrant, tetrabromoethane, into the delaminated area and insuring the penetrant completely covered this damaged area. One panel from each duplicate set was used for an x-ray by drilling a 1/2 inch hole through the delamination. The penetrant was then brushed around the hole and allowed to dissipate throughout the

delaminated area. An x-ray will show the areas covered by the penetrant as darker areas contrasted with the normal panel. Fig. 23 is a typical x-ray pattern. One will notice the different shaded areas in the delamination caused by three applications of the penetrant. However, of more importance is the edges of the delaminated area. The penetrant did not seep past the well defined circular delamination indicating no panel damage, matrix cracking, or delamination growth occurred.

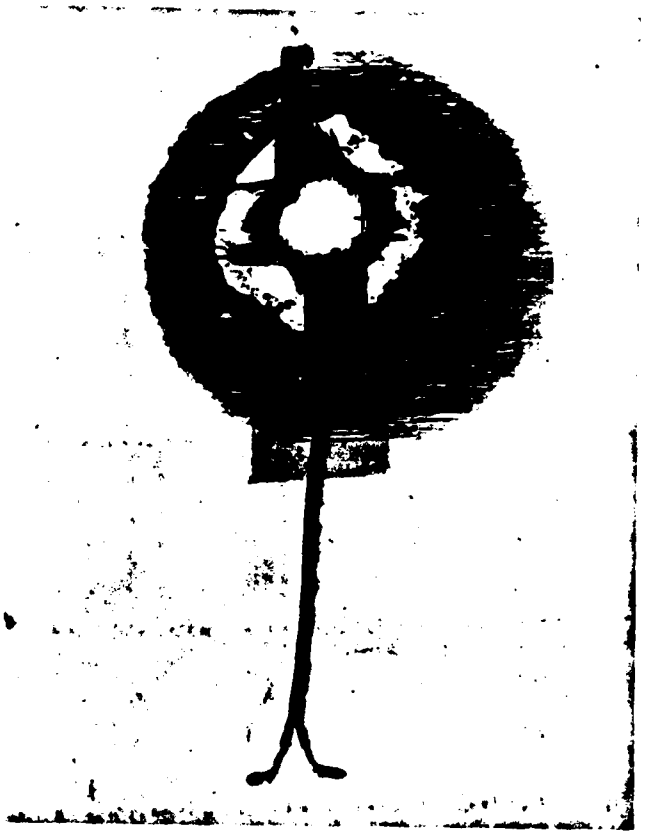

X-Ray Pattern of Panel Q221

Figure 23

Ply Orientation/Aspect Ratio Effects

Table II shows all analytical and experimental buckling loads, as well as, percent decrease in the loads for each size delamination. As was expected, the larger the size of the delamination, the less the buckling load. The $[0/-45/+45/90]_s$ orientation had the highest buckling value for panels of equal aspect ratio with no delamination, and also showed the greatest decrease in experimental values for each size delamination. This result was also expected due to the lay-up being more dependent on the $\pm$ 45 orientations in both the extensional and bending stiffness matrices. Values for all stiffness matrices are presented in Appendix B. Figures 24 and 25 graphically show the higher experimental buckling values of the quasi-isotropic lay-up with no delamination, and the greater decrease in the experimental buckling load of this lay-up as delamination size is increased, when compared to the cross-ply orientation. The vertical axis representing the buckling loads is normalized by dividing each experimental load by the largest value, which is the buckling load of the $[0/-45/+45/90]_s$ orientation with no delamination. The decrease in the load-handling capability of each panel as delamination size increases corresponds to the knockdown factors given in Table II.

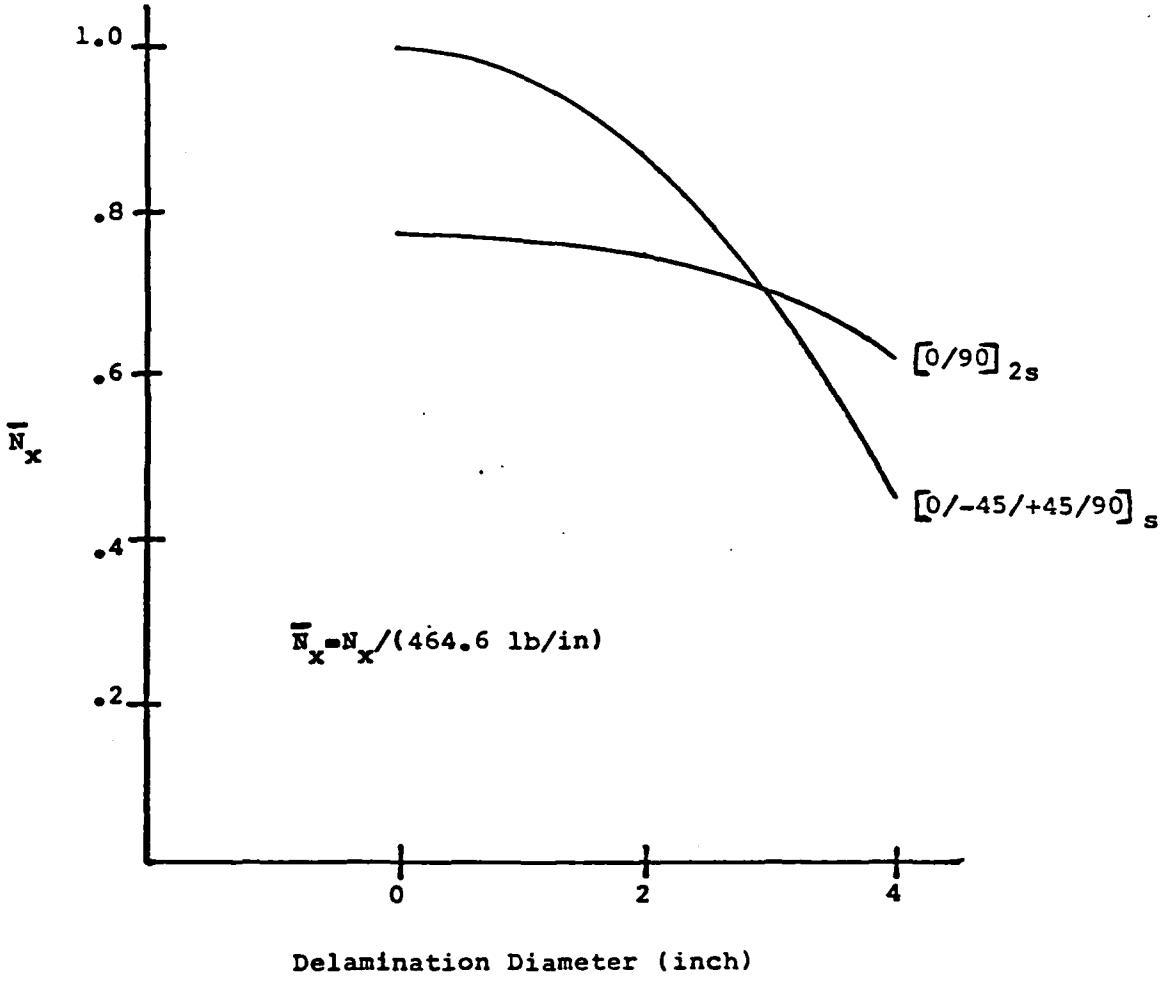

Non-Dimensionalized Experimental Values
versus Delamination Diameter AR = 1

Figure 24

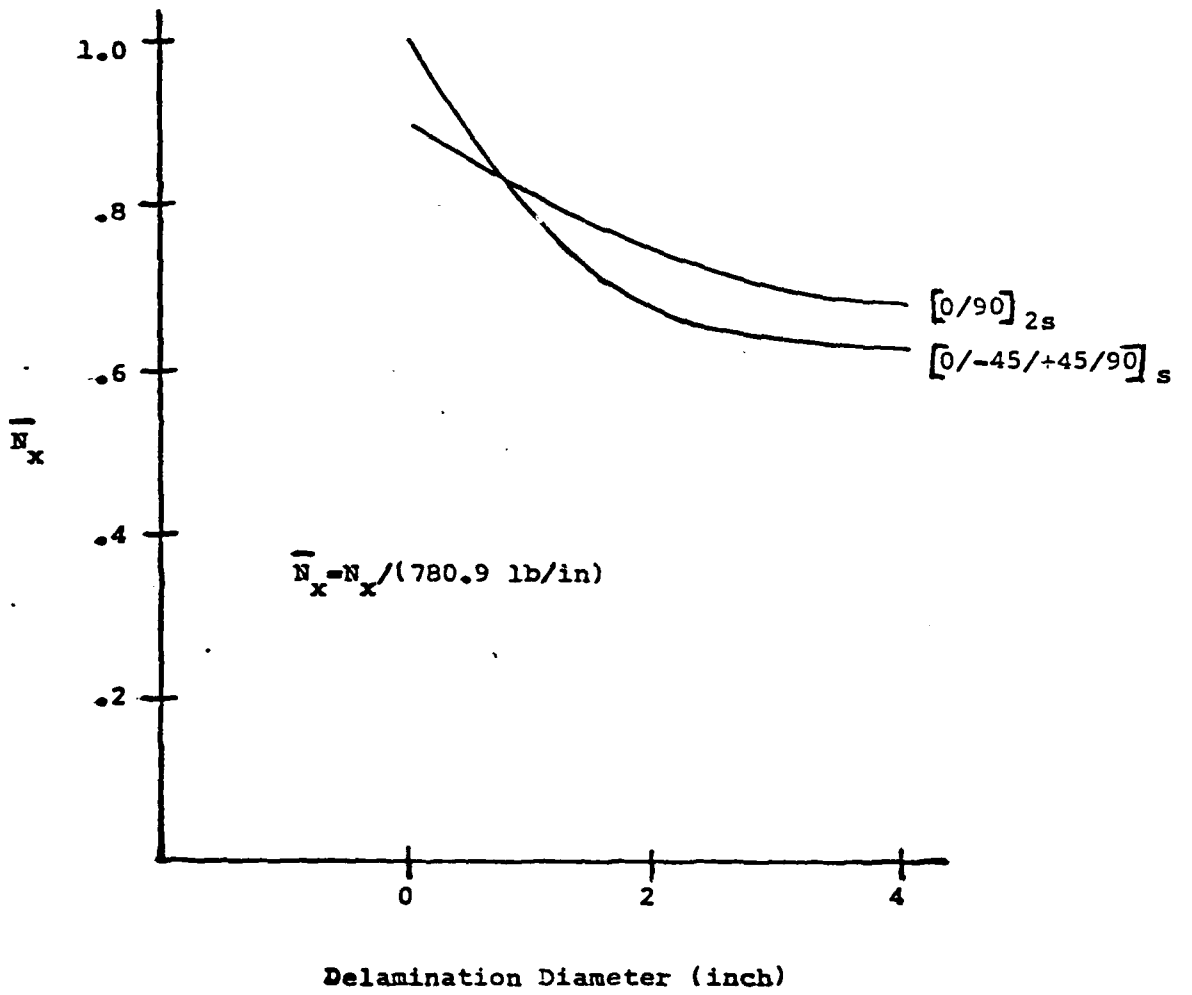

Non-Dimensionalized Experimental Values
versus Delamination Diameter AR = 1 1/2

Figure 25

The reader will note from Figures 24 and 25, the $[0/90]_{2S}$ panels become stiffer at a delamination diameter of approximately 3 inches on the panels with AR = 1 (Fig. 24), and a delamination diameter of approximately 1 inch on the panels with AR = 1 1/2 (Fig. 25). At these points, the buckling problem becomes one of the axial stiffnesses restraining the panel, rather than the bending stiffnesses that restrain a panel with no or small delaminations. Figures 16 and 17 confirm the $[0/90]_S$ panel becomes stiffer at a 3 inch delamination for panels with an AR = 1. By choosing an N_X and interpolating to a 3 inch delamination, one will find the $[0/90]_{2S}$ panel is stiffer since it allows less end-shortening. Comparing Figures 18 and 19 and interpolating to a 1 inch delamination confirms the $[0/90]_{2S}$ becomes stiffer at the 1 inch or larger delamination for an AR = 1 1/2.

Delamination/Cutout Comparison

Previous work by Janisee [9] determined the analytical collapse loads for curved panels with square cutouts. His results of a $[0/-45/+45/90]_S$ orientation and an AR = 1 are compared to the same panel with delaminations. The analytical results are; N_X = 252.1 lb/in for a 2X2 inch cutout and N_X = 113.2 for a 4X4 inch cutout for a panel with simple support conditions along the vertical sides. These values result in reduction of 56.1% and 80.3% when

compared to the analytical bifurcation load with no defects, and represent a definite lower bound to the delaminated panel since the simple support boundary conditions yield a panel that is less stiff then boundary conditions provided by the experimental fixture. The 2X2 inch cutout load is 37.6% less than the load with a 2 inch delamination, while the 4X4 inch cutout load is 46.2% less than the 4 inch delamination load.

As was previously discussed in the Analytical/Experimental Comparison section, a variety of boundary conditions along the vertical sides were modeled in the STAGSC-1 code. These results confirmed the experimental fixture did not provide the desired simple support conditions along the vertical sides, and also established an upper bound to the problem of determining the buckling load of a delaminated panel. By restraining degrees of freedom along the vertical edges, a stiffer panel with a higher bifurcation load resulted.

Three different sets of boundary conditions along the vertical sides were considered with the STAGSC-1 computer code. First, simple support conditions were modeled allowing u,v and rotation about the x-axis to be free along the entire vertical sides. A second choice restrained u and v movement, allowing only rotation. The third set of boundary conditions allowed rotation along the entire sides and u and v free along the top one inch

of the panel where the load is applied. The purpose of this third choice was to model the changing boundary conditions of the experimental fixture as the load is applied and the set screws tighten the knife edges, restraining panel movement (see Experimental Set-up). The results of these three sets of boundary conditions are:

u,v fixed	N_x = 574.0 lb/in
u, v free along top one inch	N_x = 538.1 lb/in
u,v free	N_x = 507.9 lb/in

The results of this analysis are plotted in Fig. 26 with the vertical axis, buckling load, normalized to the analytical buckling load of a perfect panel with u and v fixed along the vertical sides, N_x = 574.0 lb/in. The three values corresponding to 1.0, .94 and .88 represent the loads of the varying boundary conditions; u,v fixed, u,v free along top one inch, and u,v free, respectively. Each of these loads is for a panel with no delaminations or cutouts, hence they provide an upper bound to the delaminated panel with various boundary conditions.

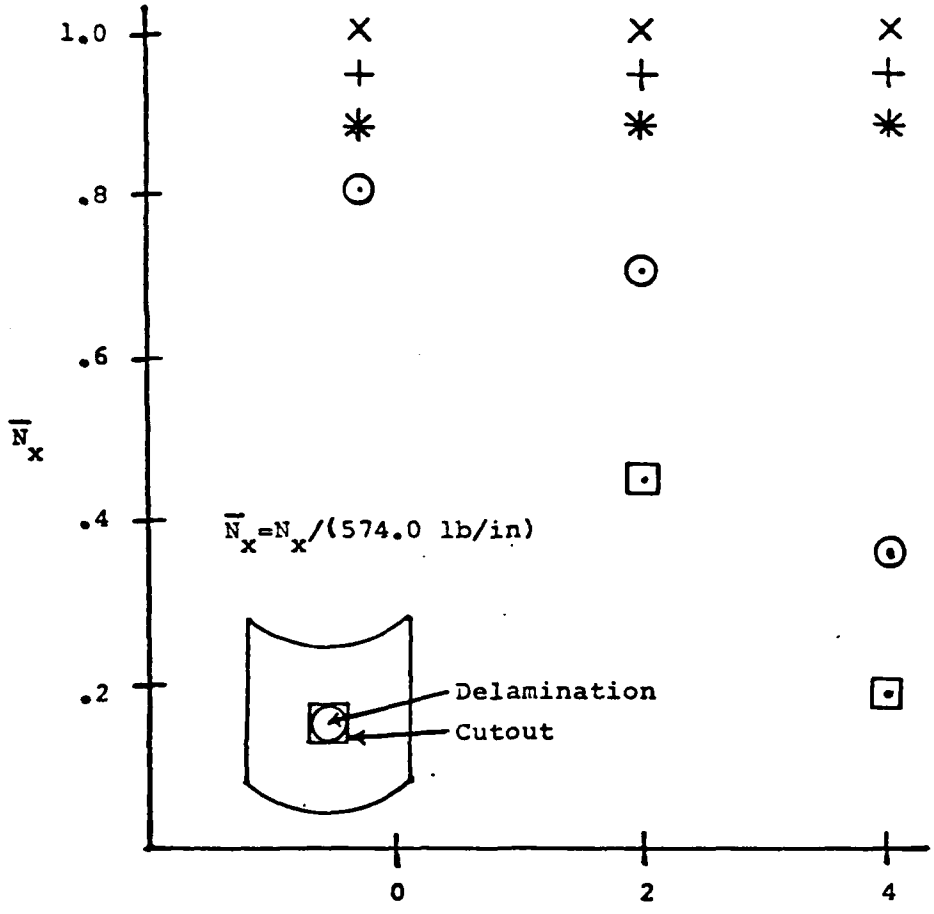

Non-Dimensionalized Buckling Load versus Defect Size
$[0/-45/+45/90]_S$ AR = 1

Figure 26

V. Conclusions

Based on the analytical and experimental results presented in this thesis, the following conclusions can be made:

1. To insure valid experimental results, the researcher must carefully choose the proper test device. When conducting experiments on axially compressed, curved composite panels, the test fixture must insure an even load application to the panel and provide the desired boundary conditions.

2. The STAGSC-1 linear analysis computes a bifurcation load for a perfect (no eccentricities or defects) panel. This load provides an upper bound for the experimental buckling load of a panel with the same ply orientation, aspect ratio, and boundary conditions. A lower bound to the experimental buckling load of a panel with a defect is provided by the STAGSC-1 analytical results of a panel with a cutout. These two results bound the experimental value of a delaminated panel with a random size and shape defect.

3. The process used to manufacture the experimental panels will effect the experimental results. Panel variations in the length, width, and thickness dimensions need to be accounted for when modeling the panel for an analytical analysis.

4. Putting a delamination at the midsurface of a curved panel allows for testing of a specimen where the delaminated layer does not separate from the panel and snap-through does not occur.

5. The delamination size effects the load-handling capability. The larger the delamination, the lower the experimental buckling load of the panel.

6. The quasi-isotropic, $[0/-45/+45/90]_S$, orientation exhibited a higher analytical and experimental buckling load than the cross-ply, $[0/90]_{2S}$, orientation for panels of the same aspect ratio and no delamination. However, for panels with the same size delamination, the quasi-isotropic panels had the greatest decrease in buckling loads and for certain delamination sizes the quasi-isotropic yielded lower loads than the cross-ply panels.

NCLASSIFIED

CLASSIFICATION OF THIS PAGE

AD-A153494

REPORT DOCUMENTATION PAGE

RT SECURITY CLASSIFICATION NCLASSIFIED	1b. RESTRICTIVE MARKINGS
RITY CLASSIFICATION AUTHORITY	3. DISTRIBUTION/AVAILABILITY OF REPORT Approved for public release; distribution unlimited.
ASSIFICATION/DOWNGRADING SCHEDULE	
RMING ORGANIZATION REPORT NUMBER(S) FIT/GAE/AA/84D-25	5. MONITORING ORGANIZATION REPORT NUMBER(S)
OF PERFORMING ORGANIZATION ool of Engineering	6b. OFFICE SYMBOL (If applicable) AFIT/EN
7a. NAME OF MONITORING ORGANIZATION	
ESS (City, State and ZIP Code) Force Institute of Technology ght-Patterson AFB, Ohio 45433	7b. ADDRESS (City, State and ZIP Code)
OF FUNDING SPONSORING NIZATION	8b. OFFICE SYMBOL (If applicable)
9. PROCUREMENT INSTRUMENT IDENTIFICATION NUMBER	
ESS (City, State and ZIP Code)	10. SOURCE OF FUNDING NOS.
(Include Security Classification) Box 19	PROGRAM ELEMENT NO. / PROJECT NO. / TASK NO. / WORK UNIT NO.
ONAL AUTHOR(S) y A. Seibert, M.S., Capt, USAF	
E OF REPORT Thesis	13b. TIME COVERED FROM _____ TO _____
14. DATE OF REPORT (Yr., Mo., Day) 1984 December	15. PAGE COUNT 81
EMENTARY NOTATION	

COSATI CODES		
	GROUP	SUB. GR.
	04	

18. SUBJECT TERMS (Continue on reverse if necessary and identify by block number)
Composites, Cylindrical Panels, Delaminations, Experimental Shell Analysis, Finite Elements, STAGSC-1, Boundary Conditions, Graphite-Epoxy

RACT (Continue on reverse if necessary and identify by block number)

tle: THE EFFECT OF CENTER DELAMINATION ON THE INSTABILITY OF COMPOSITE CYLINDRICAL PANELS

esis Advisor: Dr Anthony N. Palazotto

IBUTION/AVAILABILITY OF ABSTRACT IFIED/UNLIMITED ☒ SAME AS RPT. ☐ DTIC USERS ☐	21. ABSTRACT SECURITY CLASSIFICATION UNCLASSIFIED
E OF RESPONSIBLE INDIVIDUAL Anthony N. Palazotto	22b TELEPHONE NUMBER (Include Area Code) 513-255-3517 / 22c. OFFICE SYMBOL AFIT/EN

M 1473, 83 APR EDITION OF 1 JAN 73 IS OBSOLETE. UNCLASSIFIED

VITA

Gary R. Seifert was born on 31 March 1953 in Easton, Pennsylvania. He graduated from Souderton Area High School in 1971 and entered the United States Air Force Academy where he received a Bachelor of Science Degree in Engineering Sciences in 1975. He entered Navigator training at Mather AFB, CA and flew 7 years as an Electronic Warfare Officer in B-52G/H aircraft. He received a Master of Science Degree in Systems Management from the University of Southern California in 1982 and was accepted into the graduate Aeronautical Engineering program at the AFIT School of Engineering in 1983.

Permanent address: 412 N. Main Street
Telford, PA 18969

Similar calculations for each experimental panel showed no value of $\tilde{a}$ to exceed 3.347. Therefore, analytically, no panel would experience snap-through or delamination growth. This result was experimentally verified.

Since the experiments for this thesis applied a pure compressive load with bending strains only induced by the panel curvature, a comparison was made to the minimum value of ρ computed by Fei and Yin which was .01. By computing the value of $\tilde{a}$ for each experimental panel, it was confirmed snap-through would not occur so long as the computed value for $\tilde{a}$ did not exceed 3.347. Equation 20 is the expression for $\tilde{a}$. The value for υ was the effective laminate property computed in Appendix B. The strain in the delaminated layer, ϵ, is the strain indicated by the back-to-back strain gages centered on the delamination. The delamination depth ratio, a/h, is determined from each size delamination and a delamination depth of .022 inch.

Panel Q822

υ = .307, ϵ = 329.191 X 10^{-6}, a = 1 inch, h = .022 inch

$\tilde{a} = [12(1-\upsilon^2)\epsilon]^{1/2}$ a/h =

$[12(1-.307^2)(329.191 \times 10^{-6})]^{1/2}(1/.022)$

$\tilde{a}$ = 2.719

Panel C242

υ = .04, ϵ = 84.319 X 10^{-6}, a =2 inch, h = .022 inch

$\tilde{a} = [12(1-.04^2)(84.319 \times 10^{-6})]^{1/2}(2/.022)$

$\tilde{a}$ = 2.889

$$a\epsilon + 1/2 \int_0^a \mu^2 r^2 dr = - \int_0^a \epsilon_r dr + 1/2 \int_0^a (w')^2 dr \qquad (10C)$$

Applying (6C) to (7C) yields:

$$E\epsilon_r = \sigma_r - \upsilon\sigma_\phi = \left| -P + \upsilon(rP)' \right| / h \qquad (11C)$$

After integration by parts twice on the right hand side of (10C) and substituting (11C):

$$(1-\upsilon)\ P(a) + a\ P'(a) = Eh(\epsilon + \mu^2 a^2/6) \qquad (12C)$$

The system of four equations (7C), (8C), (9C), (12C) completely determine the functions $\phi(r)$ and $P(r)$.

However, by non-dimensionalizing the parameters, the solution to the complete buckling/postbuckling problem is reduced to the three factors: ρ, $\tilde{a}$, $\tilde{G}\tilde{a}^4$. The phenomena of snap-through is described by ρ and $\tilde{a}$ only, since their analysis found that so long as the delaminated layer maintains full contact with the main body of the plate, delamination growth can not preceed snap-through. Therefore the results of Fei and Yin can be used to determine which of the three states of the buckling/postbuckling problem a panel will experience. Their numerical results indicated that a minimum value of ρ is .01,which corresponds to a minimum $\tilde{a}$ of 3.347.

Let P(r) be the compressive radial force per unit circumferential arc length, and w(r) the transverse deflection. With the applied force, the delaminated layer will either maintain contact with the main body of the plate or buckle away from the plate, defined as snap-through. In the first case, the deformed shape of the plate is:

$$1/\mu = 1/\mu_o - H/2 \; ; \; H = t-h \qquad (5C)$$

The condition of snap-through is represented by ϕ:

$$\phi(r) = w'(r)/r \qquad (6C)$$

The P and ϕ satisfy a system of two second order non-linear differential equations:

$$r^{-3}(r^3P')' = Eh\phi^2/2 \qquad (7C)$$

$$r^{-3}(r^3\phi')' = P\phi/D \qquad (8C)$$

for $r \leq a$ and the boundary conditions at the center of the layer:

$$P'(0) = 0, \; \phi'(0) = 0 \qquad (9C)$$

Countinuity of slope along the boundary of the delamination requires w'(a) = v'(a). Also, by comparing the meridional arc lengths of the unbuckled and buckled delamination it is found:

Appendix C

Analytical Non-Dimensionalized Values

The results of the Fei and Yin [13] were used to confirm the delaminated layer would not snap-through. Their results presented snap-through states, which give the required delamination radius, $\tilde{a}$, to cause snap-through for selected values of ρ, ratio of bending deformation to membrane deformation. The analysis uses Bessel functions to express the slope and curvature of the deformed middle surface in terms of the radial coordinate, r, and the ratio of membrane force to the plate bending stiffness, λ.

$$v'(r) = A\, J_1(\lambda r) \tag{1C}$$

$$v''(r) = A\,\lambda\,[J_0\lambda(\lambda r) - (1/\lambda r) J_1(\lambda r)] \tag{2C}$$

By applying the power series expansions of Bessel functions, and assuming ($\lambda a << 1$), a small membrane force in the plate the equations simplify to:

$$v'(a) = \mu_o\, a \tag{3C}$$

$$v''(a) = \mu_o \tag{4C}$$

where $\mu_o = a\lambda/2$ is the curvature of the middle surface at the center of the plate.

$[0/-45/+45/90]_s$

$$A_{ij} = \begin{bmatrix} .361 & .111 & 0 \\ .111 & .361 & 0 \\ 0 & 0 & .125 \end{bmatrix} 10^6 \quad lb_f/in$$

$$B_{ij} = 0$$

$$D_{ij} = \begin{bmatrix} 79.867 & 12.502 & -4.884 \\ 12.502 & 21.162 & -4.884 \\ -4.884 & -4.884 & 14.392 \end{bmatrix} 10^6 \quad lb_f/in$$

$E_x = E_y = 8.172 \times 10^6$ psi

$\upsilon_{xy} = \upsilon_{yx} = .307$

$G_{xy} = 3.125 \times 10^6$ psi

$[0/90]_{2s}$

$$A_{ij} = \begin{bmatrix} .453 & .018 & 0 \\ .018 & .453 & 0 \\ 0 & 0 & .033 \end{bmatrix} 10^6 \quad lb_f/in$$

$$B_{ij} = 0$$

$$D_{ij} = \begin{bmatrix} 80.117 & 2.470 & 0 \\ 2.470 & 40.979 & 0 \\ 0 & 0 & 4.358 \end{bmatrix} 10^6 \quad lb_f/in$$

$E_x = E_y = 11.307 \times 10^6$ psi

$\upsilon_{xy} = \upsilon_{yx} = .040$

$G_{xy} = .825 \times 10^6$ psi

Appendix B

Extensional Stiffness

$$A_{ij} = \begin{bmatrix} A_{11} & A_{12} & A_{16} \\ A_{12} & A_{22} & A_{26} \\ A_{16} & A_{26} & A_{66} \end{bmatrix}$$

Coupling Stiffness

$$B_{ij} = \begin{bmatrix} B_{11} & B_{12} & B_{16} \\ B_{12} & B_{22} & B_{26} \\ B_{16} & B_{26} & B_{66} \end{bmatrix}$$

Note: For a symmetric lay-up, $B_{ij} = 0$

Bending Stiffness

$$D_{ij} = \begin{bmatrix} D_{11} & D_{12} & D_{16} \\ D_{12} & D_{22} & D_{26} \\ D_{16} & D_{26} & D_{66} \end{bmatrix}$$

Effective Laminate Properties [16]

Longitudinal Youngs' Modulus: $E_x = (A_{11}A_{22}-A_{12}^2)/tA_{22}$

Transverse Youngs' Modulus: $E_y = (A_{11}A_{22}-A_{12}^2)/tA_{11}$

Longitudinal Poissons' Ratio: $\upsilon_{xy} = A_{12}/A_{22}$

Transverse Poissons' Ratio: $\upsilon_{yx} = A_{12}/A_{11}$

Shear Modulus: $G_{xy} = A_{66}/t$

analysis is presented below.

	Density	Resin Weight (%)	Volatile Weight (%)	Void Weight (%)
Good Samples	1.6211	25.6905	.0909	.2366
Voidy Samples	1.5762	26.4328	.2400	2.8678

As can be seen from the comparison, the voidy samples were less dense in the matrix due to the higher percentage of voids. The material properties obtained from the voidy samples are:

$$E_1 = 20.82 \times 10^6 \text{ psi}$$

$$E_2 = 1.41 \times 10^6 \text{ psi}$$

$$G_{12} = .712 \times 10^6 \text{ psi}$$

$$\upsilon_{12} = .293$$

All the properties obtained from the voidy samples were less than those from the good samples. The percent decrease in values are: E_1 - .72%, E_2 - 7.84%, G_{12} - 12.64%, υ_{12} - 2.33%. The values of E_1, E_2, and υ_{12} are basically a measure of the fibers in the composite and do not show a large decrease in any of the values. However, G_{12} is determined from shear tests and a composite transfers shear stresses through the matrix. The large decrease in G_{12} is then accounted for by the voids in the matrix unable to transfer the shear.

Appendix A

This appendix presents the results of experimentally determined material properties for two identical composite lay-ups cured under different autoclave cycles. All material properties were calculated in accordance with ASTM standards. ASTM D 3039 Test for Tensile Properties of Fiber-Resin Composites was used to determine E_1, E_2, and υ_{12}. ASTM D 3518 Inplane Shear Stress-Strain Response of Unidirectional Reinforced Plastics was used to determine the shear modulus G_{12}. A total of ten samples were used for each test and the resultant material property is an average value of the ten samples.

$$E_1 = 20.97 \times 10^6 \text{ psi}$$

$$E_2 = 1.53 \times 10^6 \text{ psi}$$

$$G_{12} = .815 \times 10^6 \text{ psi}$$

$$\upsilon_{12} = .300$$

In addition to the samples used to determine the above material properties, a second set of tests were accomplished. The samples for the second test were cut from panels that were not correctly cured during the autoclave cycle. C-Scan results from these panels revealed numerous voids throughout the panels and the analysis confirmed the improper resin and void weight. A comparison of the average values from the chemical

11. Yin, W. L., Sallam, S., and Simitses, G. J., "Ultimate Axial Load Capacity of a Delaminated Plate," Proceedings of AIAA/ASME/ASCE/AHS 25th SDM Conference, Paper 84-0892, May 1984.

12. Simitses, G. J. Sallam S., and Yin W. L., "Effect of Delamination of Axially Loaded Laminated Plates, "AIAA/ASME/ASCE/AHS 25th SDM Conference, Paper 84-0964, May 1984.

13. Fei, Z., and Yin, W. L., "Post-buckling Growth of a Circular Delamination in a Laminate Under Compression and Bending," Proceedings of the Southeastern Conference on Theoretical and Applied Mechanics XII, Vol II, 130-134, May 1984.

14. Fung, Y. C., and Sechler, E. E., editors. Thin Shell Structures: Theory, Experiment, and Design. Englewood Cliffs, NJ: Prentice-Hall, Inc., 1974.

15. Buchert, Kenneth P. Buckling of Shell and Shell-Like Structures. Columbia, Missouri: K. P. Buchert and Associates, 1973.

16. Jones, Robert M., Mechanics of Composite Materials. New York: McGraw-Hill, 1975.

17. Calcote, Lee R. The Analysis of Laminated Composite Structures. New York: Van Nostrand Reinhold, 1969.

18. Almroth, B. O., Brogan, F. A., and Stanley, G. M., Structural Analysis of General Shells, Volume II User Instructions for STAGSC-1, Lockheed Palo ALto Research Laboratory, California, January 1981.

19. Litle, William A. Reliability of Shell Buckling Predictions. Cambridge, MA: The M.I.T. Press, 1964.

Bibliography

1. Bohon, Herman L. and Davis, John G. Jr., "Composites for large transports - facing the challenge," Aerospace America: 58-62, June 1984.

2. Kozichgrow, Eugene, "Air Force Funds Automatic Composite Curing System," Aviation Week and Space Technology: 71, May 14, 1984.

3. Wilkens, D. J., "Compression Buckling Tests of Laminated Graphite-Epoxy Curved Panels," AIAA Journal, 13: 465-470, April 1975.

4. Becker, M. L., Palzaotto, A. N., and Khot, N. S., "Experimental Investigation of the Instability of Composite Cylindrical Panels," Experimental Mechanics, 22: 372-376, October 1982..

5. Hebert, J. S., Analytical/Experimental Linear Bifurcation of Curved Cylindrical Composite Panels, Masters Thesis, AFIT/GAE/AA/83D-14, WPAFB, Ohio: Air Force Institute of Technology, December 1982.

6. Bauld, N. R., Jr., Experimental and Numerical Analysis of Axially Compressed Circular Cylindrical Fiber-Reinforced Panels with Various Boundary Conditions, AFWAL-TR-81-3158, WPAFB, Ohio: Air Force Wright Aeronautical Laboratories, August 1981..

7. Lee, Catherine E., Numerical Determination of the Effects of Boundary Conditions on the Instability of Composite Panels with Cutouts, Masters Thesis, AFIT/GAE/AA/83D-4, WPAFB, Ohio: Air Force Institute of Technology, December 1983.

8. Arbocz, J. and Babcock, C. D., Jr., "The Effect of General Imperfections on the Buckling of Cylindrical Shells," Journal of Applied Mechanics: 28-37, March 1969.

9. Janisse, Thomas C., A Parametric Study of Surface Imperfections and Small Cutouts in a Composite Panel, Master Thesis, AFIT/GAE/AA/82D-15, WPAFB, Ohio: Air Force Institute of Technology, December 1982.

10. Chai, H., Babcock, C. D., and Knauss, W. G., "One Dimensional Modeling of Failure in Laminated Panels by Delamination Buckling," Journal of Solids and Structures, 17: 1069-1083, November 1981.

7. Restraining boundary conditions along the vertical sides introduce a higher panel stiffness which resulted in larger buckling loads.

8. The strain-reversal and end-shortening techniques gave identical buckling loads on all panels with a delamination. This is due to the back-to-back strain gages located on the delamination which was the location of the initial buckle.

9. The knockdown factors for all panels show the same trends for each ply orientation, aspect ratio, and delamination size.

END

FILMED

6-85

DTIC